CANCER

Nonstop mutations cause loss of renal tumor suppressor proteins *VHL* and *BAP1* and affect multiple stages of protein translation

Jagriti Pal[1], Marisa Riester[1], Athina Ganner[2], Avantika Ghosh[1,3], Sonam Dhamija[1,3,4,5], Debdatto Mookherjee[6], Christian Voss[7], Ian J. Frew[8], Fruzsina Kotsis[2], Elke Neumann-Haefelin[2], Anne Spang[6], Sven Diederichs[1,3]*

Nonstop extension or stop-loss mutations lead to the extension of a protein at its carboxyl terminus. Recently, nonstop mutations in the tumor suppressor *SMAD Family Member 4* (*SMAD4*) have been discovered to lead to proteasomal SMAD4 degradation. However, this mutation type has not been studied in other cancer genes. Here, we explore somatic nonstop mutations in the tumor suppressor genes *BRCA1 Associated Protein 1* (*BAP1*) and *Von Hippel-Lindau* (*VHL*) enriched in renal cell carcinoma. For *BAP1*, nonstop mutations generate an extremely long extension. Instead of proteasomal degradation, the extension decreases translation and depletes *BAP1* messenger RNA from heavy polysomes. For *VHL*, the short extension leads to proteasomal degradation. Unexpectedly, the mutation alters the selection of the translational start site shifting VHL isoforms. We identify germline *VHL* nonstop mutations in patients leading to the early onset of severe disease manifestations. In summary, nonstop extension mutations inhibit the expression of renal tumor suppressor genes with pleiotropic effects on translation and protein stability.

INTRODUCTION

Nonstop mutations, also known as stop-loss, stop-lost mutations, readthrough, or nonstop extension (NSExt) mutations, cause conversion of a stop codon into a sense codon. This alteration directs translation into the 3′ untranslated region (3'UTR) of the messenger RNA (mRNA) until the next in-frame stop codon, resulting in the extension of the protein at its C terminus (Fig. 1A). When the translation machinery does not encounter a second stop codon, it reaches the poly-A sequence of the mRNA, a phenomenon called translation readthrough, leading to the degradation of the mRNA via the no-stop-decay (*1*, *2*).

Across species, from worms to humans, translation past the normal stop codon has been shown to often be detrimental to protein expression (*3*–*5*). Bioinformatic analyses have shown that 99% of human mRNAs have in-frame stop codons in the 3'UTR (*5*). This implies that mutations in the stop codon of the human proteome could give rise to newly created C termini with potentially pathological consequences. Nonstop mutations have been studied in various hereditary disorders (*6*), e.g., affecting the *Integral Membrane Protein 2B* (*ITM2B*, a.k.a. *BRI*) gene in British familial dementia (*7*, *8*), *Melanocyte Inducing Transcription Factor* (*MITF*) in Waardenburg syndrome (*9*), *Receptor Accessory Protein 1* (*REEP1*) in peripheral neuropathy (*10*), and *Thymidine Phosphorylase* (*TYMP*) in mitochondrial neurogastrointestinal encephalomyopathy (*11*). These extended mutant proteins are dysregulated through degradation (*5*), mislocalization (*9*), misfolding and aggregation (*10*), or aberrant modifications (*12*).

In the field of cancer genetics, the functional implications of nonstop mutations have largely been overlooked with substantial focus given to understanding missense and nonsense point mutations (*13*). Some studies have merely mentioned the presence of nonstop mutations in cancer samples without investigating their functional consequences (*14*–*17*). Dhamija *et al.* (*18*) undertook the first endeavor to unravel the functional consequences of nonstop mutations in the tumor suppressor gene *SMAD Family Member 4* (*SMAD4*). The NSExt mutations in *SMAD4* occurred specifically in pancreatic, colon, and bile duct cancers, which are known to be driven by other types of SMAD4 protein loss (*19*–*21*). The mutations induced a loss-of-function phenotype through the translation of a hydrophobic degron sequence at the C terminus, resulting in robust and rapid proteasomal degradation of the extended protein. Thus, this work demonstrated the profound functional significance of nonstop mutations in cancer, highlighting the importance of studying their mechanisms underlying tumorigenesis. Moreover, NSExt mutations in the tumor suppressor gene *Phosphatase and Tensin Homolog* (*PTEN*) also gave rise to proteasomal degradation due to a C-terminal hydrophobic extension (*22*).

Previously, we have also generated a comprehensive database for somatic nonstop mutations in cancer called NonStopDB (*18*, *23*), which provides pan-cancer data of thousands of nonstop mutations from the Catalog of Somatic Mutations in Cancer (COSMIC v89) across 96 distinct tumor types (as annotated by COSMIC). In the present study, we explored further tumor entities and cancer-associated genes recurrently altered by nonstop mutations. The analysis revealed nonstop mutations in the tumor suppressor genes *Von Hippel-Lindau* (*VHL*) and *BRCA1-Associated Protein 1* (*BAP1*) to be enriched in

[1]Division of Cancer Research, Department of Thoracic Surgery, Medical Center - University of Freiburg, Faculty of Medicine, University of Freiburg, Freiburg, Germany. [2]Renal Division, Department of Medicine, Medical Center - University of Freiburg, Faculty of Medicine, University of Freiburg, Freiburg, Germany. [3]German Cancer Consortium (DKTK), partner site Freiburg, a partnership between DKFZ and University Medical Center, Freiburg, Germany. [4]CSIR-Institute of Genomics and Integrative Biology, New Delhi, India. [5]Academy of Scientific and Innovative Research (AcSIR), Ghaziabad, Uttar Pradesh, India. [6]Biozentrum, University of Basel, Basel, Switzerland. [7]Department of Radiology, Medical Center - University of Freiburg, Faculty of Medicine, University of Freiburg, Freiburg, Germany. [8]Department of Internal Medicine I, Medical Center - University of Freiburg, Faculty of Medicine, University of Freiburg, Freiburg, Germany.
*Corresponding author. Email: s.diederichs@dkfz.de

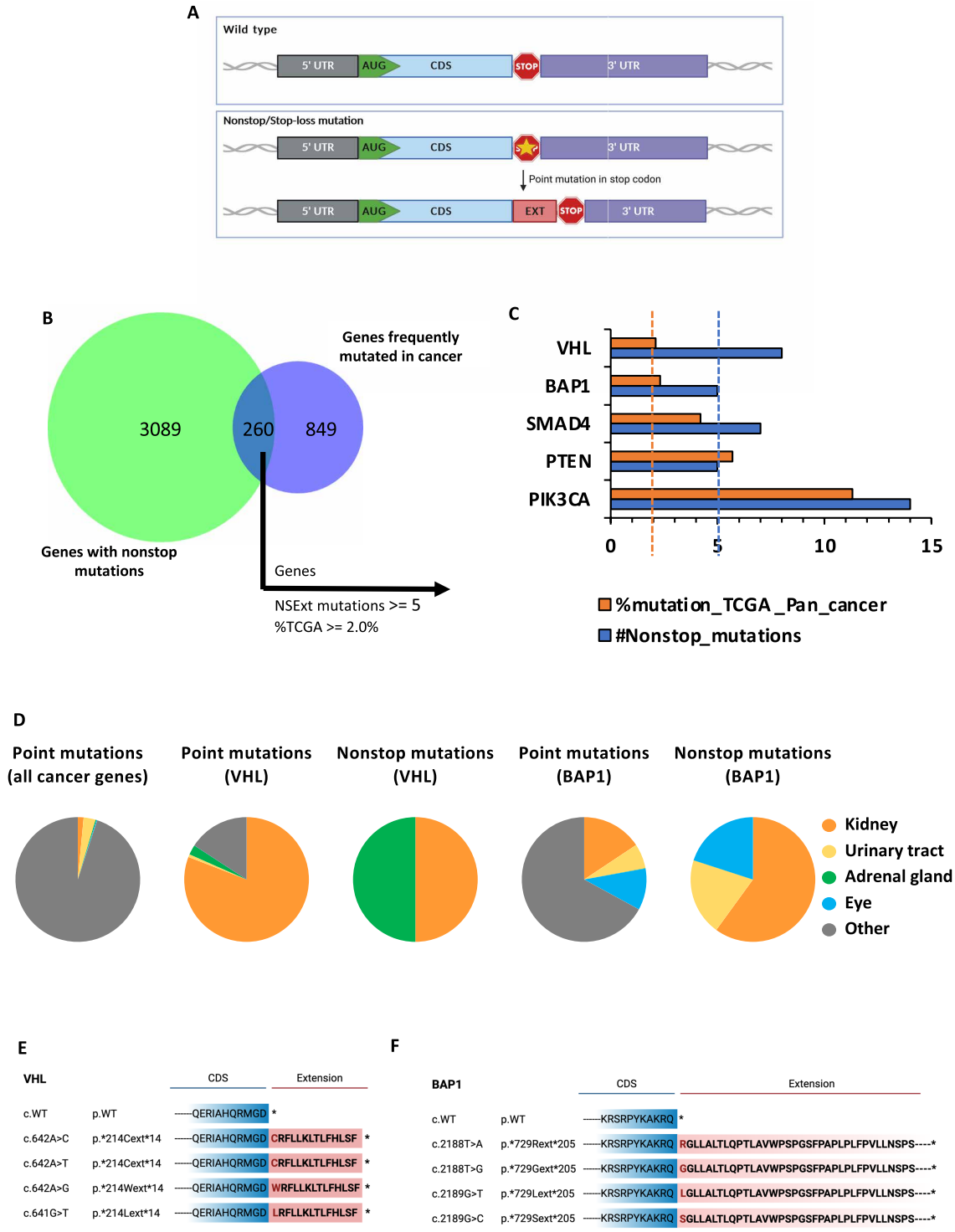

Fig. 1. Recurrent nonstop mutations in tumor suppressor genes *BAP1* and *VHL* in kidney cancer. (**A**) Schematic view of nonstop (NSExt) or stop-loss mutations. Created in BioRender. Pal (2024); https://BioRender.com/z76o007. (**B**) Overlap of genes harboring nonstop mutations (COSMIC v98) with genes frequently mutated across all tumor entities (PANcancer) from The Cancer Genome Atlas (TCGA). (**C**) Number of nonstop mutations (blue) versus frequency of mutation in TCGA PANcancer data (orange) for the genes selected from (B). The blue line represents the threshold of five nonstop mutations and the orange line represents the threshold of 2% mutation frequency in TCGA PANcancer data. (**D**) Frequency distribution according to the primary site of the tumor for all point mutations in all Cancer Gene Census coding sequences in COSMIC v98, in *VHL* or in *BAP1* in comparison to the entities with nonstop extension mutations in these two genes. (**E**) Representation of the four different nonstop mutations in the VHL gene occurring eight times in COSMIC. (**F**) Representation of the four different nonstop mutations in the BAP1 gene occurring five times in COSMIC. Created in BioRender. Pal (2024); https://BioRender.com/o34m945 (E and F).

kidney cancer. We show that nonstop mutations in both genes led to loss of protein expression, but importantly, via different mechanisms affecting not only protein stability but also multiple steps of translation.

RESULTS

Tumor suppressor genes *VHL* and *BAP1* harbor nonstop mutations in kidney cancer

To identify nonstop mutations of potential functional relevance in cancer, we searched for all nonstop mutations in a pan-cancer analysis. In COSMIC v98 (*24*, *25*), a total of 3349 genes harbored nonstop mutations in cancer; 260 of these genes were concurrently frequently affected by point mutations (e.g., missense) according to The Cancer Genome Atlas (TCGA) pan-cancer mutation data (*26*–*29*) (Fig. 1B). Of these 260 genes, 5 genes—*phosphatidylinositol-4,5-bisphosphate 3-kinase catalytic subunit alpha* (*PIK3CA*), *PTEN*, *SMAD4*, *VHL*, and *BAP1*—had recurrent nonstop mutations in five or more patients (NonStopDB) and concomitantly were mutated in more than 2% of cancers in the TCGA pan-cancer point mutation data (Fig. 1C), indicating their potential importance in tumorigenesis. Notably, four of these five genes (*VHL*, *BAP1*, *SMAD4*, and *PTEN*) were tumor suppressor genes according to the Cancer Gene Census v98 (*24*, *25*), while only PIK3CA was categorized as an oncogene reflecting again the enrichment of nonstop mutations in tumor suppressor genes (*18*). Next, we aimed to identify nonstop mutations specifically enriched in tumor entities that were frequently also affected by other types of mutations in the same respective genes. Previously, we had found the functionally important *SMAD4* nonstop mutations specifically in tumors of the digestive system like pancreatic and colon cancer, which were known to be driven by loss of SMAD4 (*18*). Here, we identified nonstop mutations in two of the genes to be specifically enriched in kidney cancer, *VHL* and *BAP1*, in which also other point mutations were tissue-specifically enriched (Fig. 1D). Hence, we focused on these tumor-specific nonstop mutations in *VHL* and *BAP1*, because these are also known key tumor suppressor genes in kidney cancer (*30*). Furthermore, *VHL* nonstop mutations were found in pheochromocytoma of the adrenal gland, which is a known VHL-driven disease. For *BAP1*, many point mutations were also found in uveal melanoma of the eye, where also one of the nonstop mutations was found (Fig. 1D).

The tumor suppressor protein VHL is a part of an E3-ubiquitin ligase complex and is involved in hypoxia-related cellular signaling pathways (*31*). Inactivating point mutations, indels, and gene deletions of the gene have been implicated in the VHL syndrome where patients present with tumors in kidneys, adrenal glands, central nervous system (CNS), pancreas, and reproductive organs (*32*). From NonStopDB, we identified three different nonstop mutations in *VHL* in eight patients, of whom four had a malignant kidney cancer, while the other four had pheochromocytoma (Fig. 1E and table S1). The mutations gave rise to a 14–amino acid extension sequence (Fig. 1E).

The tumor suppressor protein BAP1, a.k.a., ubiquitin carboxyl-terminal hydrolase, is a member of the deubiquitinase family of proteins and inactivating somatic mutations and deletions in the gene have been linked to clear cell renal cell carcinoma (ccRCC), uveal melanoma, and mesothelioma (*33*, *34*). We found four different nonstop mutations in five patients, three of whom were ccRCC, one was uveal melanoma, and another was bladder carcinoma (Fig. 1F and table S1). The nonstop mutation in *BAP1* resulted in a 205–amino acid–long extension sequence, the longest in a cancer gene census gene in the NonStopDB.

To study the biological consequence of nonstop mutations in *VHL* and *BAP1*, we generated endogenously mutated human embryonic kidney (HEK) 293 cell lines via precision genome editing using two CRISPR-Cas systems (fig. S1A), *Streptococcus pyogenes* (Sp) Cas9 for *BAP1* and *Acidaminococcus* sp. (As) Cas12 for *VHL* based on protospacer adjacent motif (PAM) sequence availability and differential homology-directed repair (HDR) efficiency. To exclude clone-specific effects, multiple clones of each mutation were cultivated and analyzed. The wild-type (WT) and homozygous nonstop mutant cell lines were confirmed using Sanger sequencing (fig. S1, B and C).

Nonstop mutations in *BAP1* lead to protein loss due to decreased translation

We generated three WT clones and three clones each harboring one of the four nonstop mutations (Stop>Glycine or *>G, Stop>Leucine or *>L, Stop>Arginine or *>R, and Stop>Serine or *>S) in HEK293 cells (fig. S1, A and B). Analysis of the mRNA levels revealed no significant difference between the nonstop mutant *BAP1* mRNA and the WT clones (Fig. 2A). However, the nonstop mutant proteins were almost undetectable (Fig. 2B and fig. S2A). The BAP1 protein is the hydrolase component of the Polycomb repressive complex and catalyzes the removal of the ubiquitin moiety from histone H2A at lysine-119 (K119) (*35*). Loss of BAP1 in the mutant cell lines led to a significant increase in the ubiquitination levels of H2A-K119 (Fig. 2B).

To evaluate whether, similar to SMAD4, the loss of the BAP1 protein was due to its degradation, we inhibited either the ubiquitin proteasome pathway using bortezomib (Bort.) or MG132 or the endo-lysosomal pathway using chloroquine (Chlor.) or bafilomycin A1 (BafA1) and tested for protein rescue. The inhibition of neither pathway rescued the loss of the mutant (NSExt) BAP1 protein (Fig. 2C). In addition, treatments with a panel of protease inhibitors, such as a protease inhibitor cocktail, phenylmethylsulfonyl fluoride, calpeptin, PD15606, bestatin, batimastat, the E3 ligase complex inhibitor GS143, or the ubiquitination inhibitor TAK243 as well as the combination of ubiquitin-proteasome and endo-lysosomal pathway inhibitors (bortezomib + bafilomycin A1) could not rescue NSExt BAP1 protein expression (fig. S2B), suggesting a degradation-independent mechanism of protein loss.

Because loss of the NSExt-mutant BAP1 protein was apparently not due to its degradation, we hypothesized that a translational regulation could cause the decrease in protein expression. The *BAP1* gene has an in-frame second open reading frame (ORF) downstream in its 3'UTR coding for a predicted 162–amino acid HUCEP13 protein (UniProt ID: Q96TC6), which corresponds to the latter part of the 205–amino acid extension sequence (fig. S3A). Translation of downstream ORFs in the 3'UTR could potentially affect translation of the canonical ORF (*36*). Thus, the presence of an NSExt mutation in *BAP1* could lead to an interaction or interference between the translation machinery on the BAP1 extension and the overlapping translation initiation site of the downstream ORF of HUCEP13. Hence, we created an expression construct containing the *BAP1* cDNA along with its extension sequence, and either mutated the start codon or deleted the KOZAK sequence of the HUCEP13 ORF. The mutation of the translational start sequence of HUCEP13 did not alter the expression of the BAP1 ORF from this exogenous

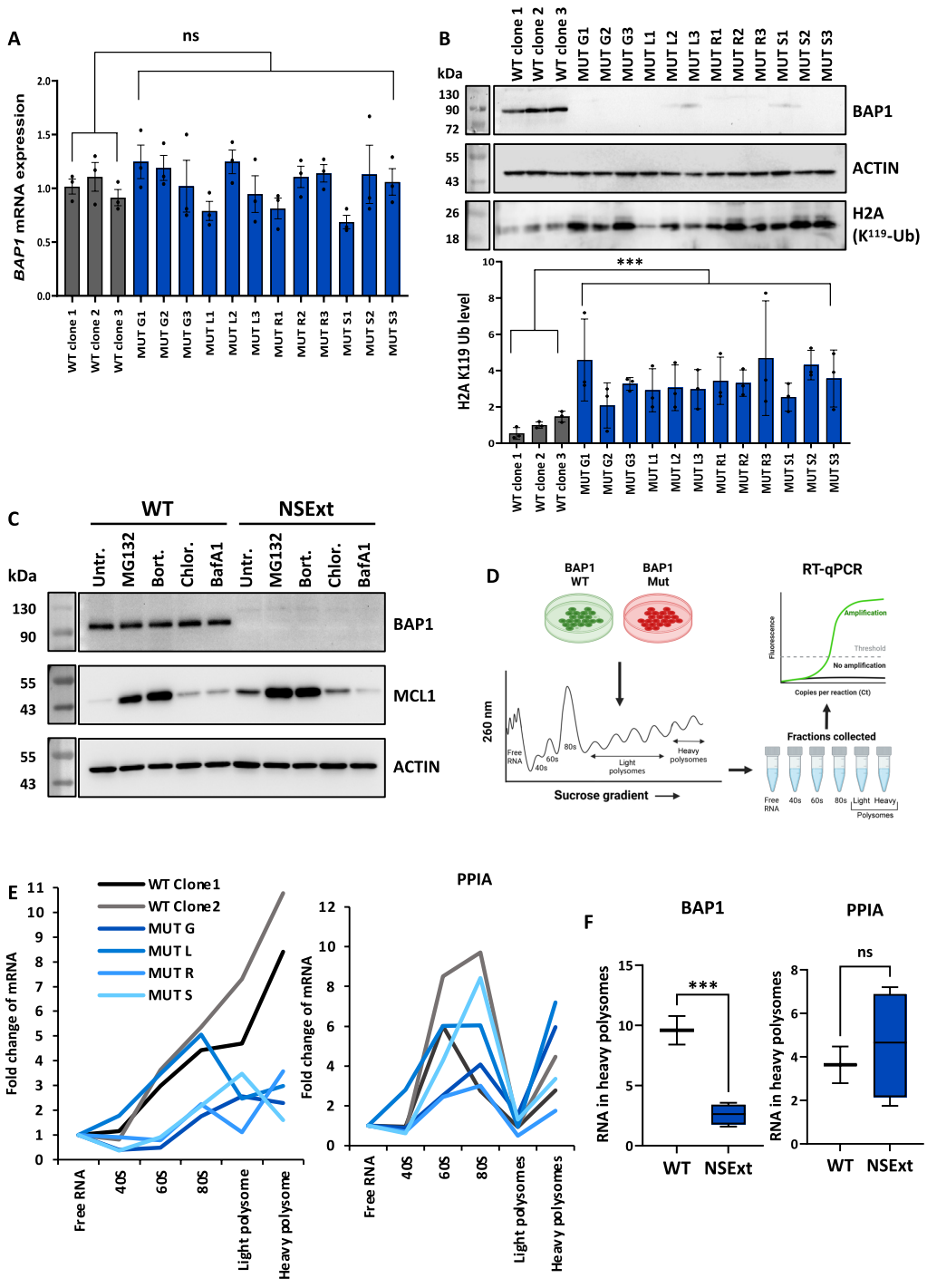

Fig. 2. Nonstop mutations in *BAP1* lead to loss of the protein via reduced translation. (**A**) *BAP1* mRNA levels ($N = 3$) in HEK293 cells with endogenously either wild-type (WT, gray) or nonstop mutant (MUT, blue) *BAP1* created by precision genome editing. G, L, R, and S refer to the change from stop codon to Gly, Leu, Arg, and Ser, respectively. WT clone refers to HEK293 clones generated from CRISPR-Cas experiments. The numbers identify the different homozygous clones for each genotype to exclude clone-specific differences. (**B**) BAP1 protein levels were reduced in MUT versus WT clones, while the ubiquitination of its downstream target histone H2A at K119 was increased ($N = 3$). (**C**) Treatment of WT and NSExt (MUT G1) HEK293 cells showed no rescue of the mutant protein with neither ubiquitin-proteasomal [MG132 and bortezomib (Bort.)] nor endo-lysosomal [chloroquine (Chlor.) and bafilomycin A1 (BafA1)] inhibitors ($N = 3$). MCL1 served as positive control for proteasomal inhibition. Untr. refers to untreated cells, i.e., 0.8% DMSO, which is the highest DMSO concentration used for the drugs. (**D**) Schematic workflow of polysome fractionation and RT-qPCR for *BAP1*. Created in BioRender. Pal (2024); https://BioRender.com/a30l718. (**E**) RT-qPCR quantification of the mRNA expression of *BAP1* and *PPIA* as control mRNA in WT and mutant cells after polysome fractionation. The fold changes were calculated relative to the free RNA fractions. Here, error bars for individual values are not shown for ease of visualization ($N = 3$). (**F**) Comparison of the RNA abundance in the heavy polysome fractions for *BAP1* and *PPIA* mRNAs normalized to their abundance in free RNA. For (A), (B), and (F), an *F* test followed by an unpaired *t* test was performed where ns and *** refer to *P* values of >0.05 and <0.001, respectively.

expression construct (fig. S3B). To exclude the idea that the exogenous overexpression might conceal any possible impact of the HUCEP13 translational start region, we endogenously mutated the start codon of the *HUCEP13* gene in the *BAP1* gene locus via precision genome editing. The endogenous start site mutation of *HUCEP13* also did not alter the expression of either the WT or the NSExt BAP1 protein (fig. S3C). Thus, the presence of the second ORF HUCEP13 in the 3'UTR of *BAP1* did not influence the translation of the BAP1 protein. Furthermore, we tested whether the knockdown of proteins involved in the ribosome-associated quality control like endothelial differentiation-related factor 1 (EDF1, a stabilizer of Grb10-Interacting GYF Protein 2 or GIGYF2), eukaryotic translation initiation factor 4E family member 2 (EIF4E2, a.k.a. 4EHP), E3 ubiquitin ligase zinc finger protein 598 (ZNF598), nuclear export mediator factor (NEMF), or E3 ubiquitin protein ligase listerin 1 (LTN1) could rescue the loss of the extended BAP1 protein (*37*–*39*). However, these did not show any effect on the protein expression level of the NSExt BAP1 protein (fig. S3, D and E). In addition, we performed semiquantitative reverse transcription polymerase chain reaction (RT-PCR) on RNA isolated from WT and NSExt *BAP1* cells and analyzed the resulting amplicons around the mutated stop codon or upstream or downstream of it by gel electrophoresis but did not find any evidence for RNAs of aberrant sizes or amounts that could have indicated a potential effect on cryptic splice sites around the stop codon (fig. S3F).

Next, we evaluated the effect of *BAP1* mutations on its translation using the rabbit reticulocyte in vitro transcription-translation system. We observed a partial but significant reduction in the translation capacity of all four NSExt BAP1 ORFs compared to the WT ORF containing the extension sequence with a normal stop codon (fig. S3, G and H). To further corroborate the translational impact of the NSExt mutations, we analyzed the distribution of *BAP1* mRNA in the different translational complexes to compare their capacities to undergo translation. Using a sucrose gradient for polysome profiling, we isolated free RNA, 40S, 60S, 80S, light polysome, and heavy polysome fractions from WT and NSExt HEK293 cells. We then quantified the distribution of *BAP1* mRNA and a control mRNA, *Cyclophilin A* (*PPIA*), in the different fractions (Fig. 2D). *BAP1* mRNA was significantly depleted in the heavy polysome fraction in all four nonstop mutant cell lines compared to both WT clones (Fig. 2, E and F). This pattern was not observed for the control *PPIA* mRNA. Thus, the loss of BAP1 protein in the nonstop mutant cell lines was associated with a substantial reduction in the effective translation of the mutant mRNAs.

Nonstop mutations in *VHL* cause proteasomal degradation of the tumor suppressor protein

The *VHL* locus in HEK293 cells was altered with precision genome editing using the CRISPR-Cas12 system to endogenously introduce the nonstop mutations (fig. S1, A and C). One parental WT and one clonal WT from the mutagenesis experiment served as controls, and two clones for each of the three nonstop or NSExt mutations (Stop>Cysteine or *>C, Stop>Tryptophan or *>W, and Stop>Leucine or *>L) were used for further analysis. Similar to what we have observed for BAP1 above, the introduction of the nonstop mutation showed no significant alteration in the *VHL* mRNA levels (Fig. 3A), but led to a significant and almost complete loss of the NSExt VHL protein (Fig. 3B and fig. S4A). VHL functions in the ubiquitination and degradation of hypoxia-inducible factor α subunits (HIF-αs), a class of transcription factors that play a central role in gene regulation in response to oxygen levels (*40*). In the NSExt cell lines, the loss of VHL protein caused an increase in transcription factor HIF-1α protein abundance (Fig. 3, B and C). Concurrently, many target genes of HIF-1α including *Vascular Endothelial Growth Factor A* (*VEGFA*), *Vascular Endothelial Growth Factor C* (*VEGFC*), *Fms Related Receptor Tyrosine Kinase 1* (*FLT-1*), *Heme Oxygenase 1* (*HMOX1*), *Phosphoglycerate Kinase 1* (*PGK1*), *Cadherin 2* (*CDH2*), *Snail Family Transcriptional Repressor 2* (*SNAI2*), *Zinc Finger E-Box Binding Homeobox 1* (*ZEB1*), and *Vimentin* (*VIM*) increased at the mRNA level (Fig. 3D and fig. S4, B to G), verifying the loss of VHL activity in the NSExt mutant cells. At the cellular level, the NSExt mutant cell lines displayed an increased capacity of migration compared to the WT cell lines (Fig. 3E) while both long-term colony formation and short-term proliferation remained unaffected (fig. S5, A to C), matching previous observations of the cellular phenotype of VHL loss (*41*). Last, the loss of the protein was not due to aggregation (*42*), as neither the WT nor the NSExt protein was detected in the insoluble fraction of the cell lysate (fig. S5D).

We next tested for protein degradation. The VHL WT and NSExt cells were treated with inhibitors of either the ubiquitin-proteasome pathway bortezomib (Bort.) or MG132 or of the endo-lysosomal pathway chloroquine (Chlor.) or bafilomycin A1 (BafA1). Western blot analysis revealed that the abundance of the NSExt VHL protein was strongly rescued upon inhibition of the ubiquitin-proteasome pathway (Fig. 3, F and G). To further evaluate the impact of protein stability on the protein loss caused by VHL NSExt mutations, we determined the stability of the WT and mutant proteins through the cycloheximide (CHX) chase method. Although the NSExt VHL protein was briefly stabilized by treatment with bortezomib at the beginning of the chase, the protein was quickly degraded with a half-life of only ~4.5 hours as compared to WT VHL, which displayed a much longer half-life of ~20 hours (Fig. 3, H to J). Thus, nonstop mutations in VHL lead to decreased protein stability and a rapid degradation of the protein via the ubiquitin-proteasome pathway, resulting in increased HIF-1α signaling and increased migration capacity.

Previously, a hydrophobic degron was identified in the SMAD4 C-terminal extension (*18*), and more generally, C-terminal extensions degraded by the proteasomal machinery were observed to be enriched in hydrophobic residues (*43*). This prompted us to evaluate the hydrophobicity of the C-terminal amino acids of the nonstop mutant VHL, which revealed that compared to the C terminus of the WT protein, the NSExt protein had an increased hydrophobicity based on both the Kyte-Doolittle and the Miyazawa hydrophobicity scales. The cumulative median hydrophobicity scores of the last 14 amino acids of the VHL protein switched from hydrophilic in WT to hydrophobic in the mutant (fig. S6, A and B). Conversely, neither this strong increase in hydrophobicity nor the switch to overall hydrophobicity was observed for the C terminus of the BAP1 nonstop protein, for which the protein loss occurred through translation inhibition (fig. S6, C and D).

Mutations in the stop codon of *VHL* cause alternative start site selection

In the presence of proteasome inhibitors, we observed that the introduction of NSExt mutations differentially affected the abundance of different protein isoforms of VHL (Fig. 3F). The *VHL* gene codes for two major protein isoforms, VHL^{213} and VHL^{160}. The VHL^{213}

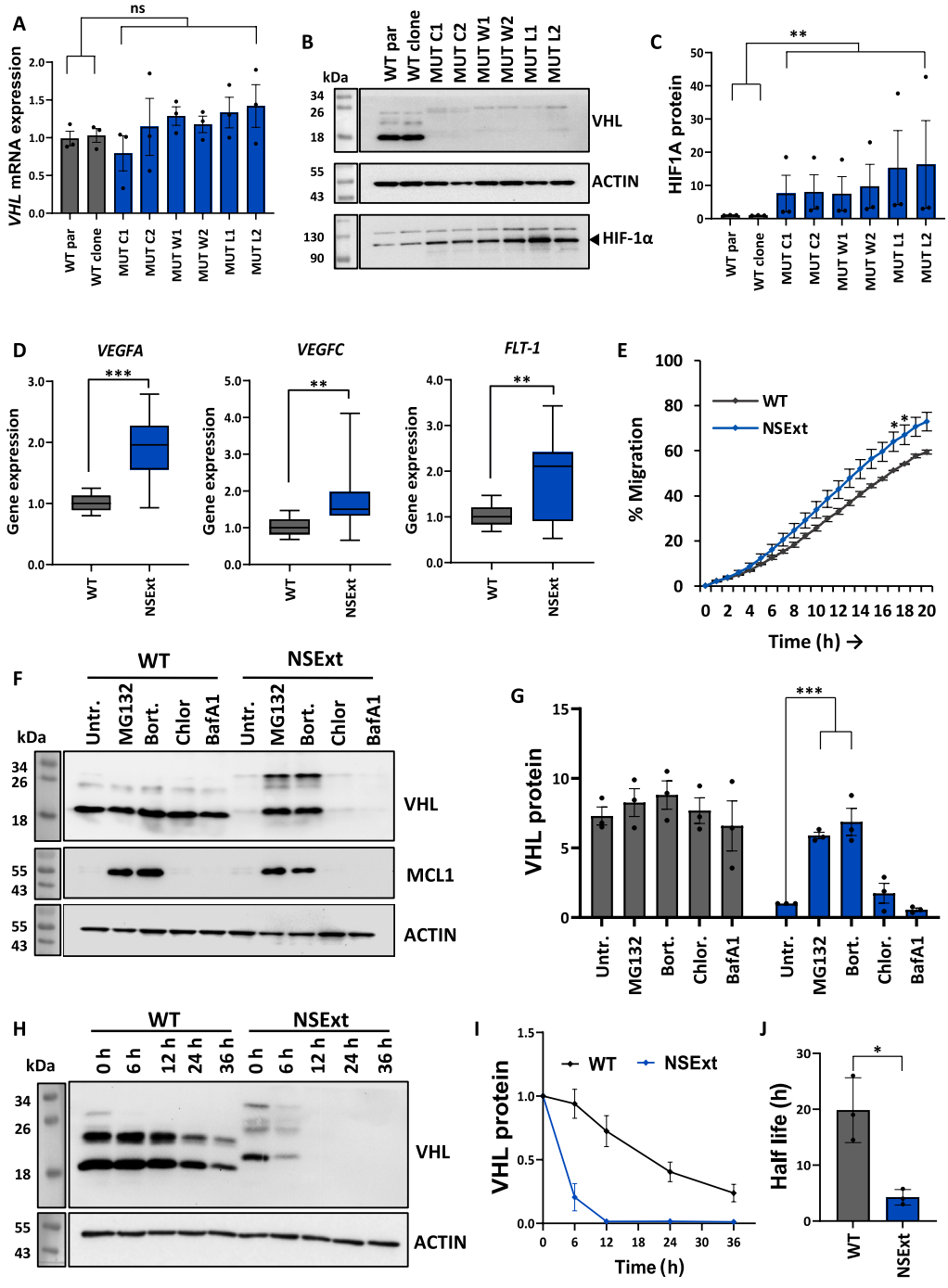

Fig. 3. Nonstop mutations in *VHL* lead to loss of the protein via the ubiquitin-proteasome pathway. (**A**) *VHL* mRNA levels in HEK293 cells with wild-type (WT, gray) or nonstop mutant (MUT, blue) *VHL* created by precision genome editing ($N = 3$). WT par refers to parental HEK293 cells, while WT clone refers to a WT HEK293 clone obtained during the CRISPR-Cas–mediated mutagenesis of the *VHL* locus. C, W, and L refer to the stop codon change to Cys, Trp, and Leu, respectively. The numbers identify the different homozygous clones for each genotype to exclude clone-specific differences. (**B** and **C**) Reduced VHL and increased downstream target HIF-1α protein levels in MUT versus WT cells [quantification in (C), $N = 3$]. (**D**) Mutant cells (NSExt and MUT C2) displayed an increase in mRNA levels of HIF-1α downstream targets *VEGFA*, *VEGFC*, and *FLT-1* ($N = 3$). (**E**) Mutant cell lines (NSExt) showed increased migration capacity in an IncuCyte Wound Healing assay ($N = 4$). h, hours. (**F** and **G**) Treatment of WT versus NSExt (MUT C2) HEK293 cells with ubiquitin-proteasomal pathway inhibitors [MG132 and bortezomib (Bort.)] led to a rescue of the mutant VHL protein, but not with endo-lysosomal pathway inhibitors [chloroquine (Chlor.) and bafilomycin A1 (BafA1)] [quantification in (G), $N = 3$] with MCL1 serving as a positive control for proteasomal inhibition. Untr. refers to untreated cells, i.e., 0.8% DMSO, which is the highest DMSO concentration used for the drugs. (**H** to **J**) Cycloheximide chase experiments unraveled reduced half-life of mutant VHL (NSExt and MUT C2). Both WT and NSExt cells were treated with 0.1 μM bortezomib for 8 hours followed by cycloheximide treatment. After adding the cycloheximide, cells were collected at 0, 6, 12, 24, and 36 hours ($N = 3$). For (A), (C), (D), (E), (G), and (J), an *F* test followed by an unpaired *t* test was performed. Here, ns, *, **, and *** refer to *P* values of >0.05, <0.05, <0.01, and <0.001, respectively.

isoform is composed of 213 amino acids. The smaller isoform, VHL^{160}, results from an alternative translation initiation site at codon 54 in the ORF, resulting in a protein of 160 amino acids, thus lacking the first 53 residues (*44*). Both start site isoforms could be important for tumor suppressor effects of the VHL gene (*44*).

A third isoform, VHL^{172}, arises from a transcript variant resulting from alternative splicing lacking the second exon (fig. S7A—only depicting the longer VHL^{213} and shorter VHL^{172} transcript isoforms resulting from alternative splicing). This isoform does not function as a tumor suppressor gene (*45*). The VHL^{213} isoform remained unchanged (fig. S7B). The VHL^{172} splicing isoform was reduced at the RNA level, but this effect was not seen consistently in all of the nonstop mutant clones (fig. S7C).

For the isoforms based on translational start site selection, VHL^{213} and VHL^{160}, we observed a strong shift in the amount of the two protein isoforms compared to the WTs when we rescued the nonstop mutant VHL protein using bortezomib; i.e., the amount of VHL^{213} was significantly higher in the mutants than in the WTs (Fig. 4, A and B). Because this change in translation start site selection by a mutation in the stop codon was a surprising observation, we further investigated this phenomenon. The recognition of a start codon and the start of translation are determined by cis-acting translation initiation signals and trans-acting RNA-binding protein factors (*46*). We hypothesized that the stop codon mutation in VHL could affect the composition of these factors on the mRNA resulting in the altered start codon selection from primarily VHL^{160} in WT cells to almost equal levels of VHL^{213} and VHL^{160} in NSExt mutant cells (Fig. 4A). We performed an RNA affinity purification to pull down *VHL* mRNA with its bound protein complexes from WT and NSExt mutant cell lines and identified the bound proteins by mass spectrometry (RAP-MS) (Fig. 4C). We identified 63 annotated, noncontaminant proteins that were detected by at least five peptides, occurred in two or three replicates of one genotype (WT or NSExt), and were absent in the respective other genotype and showed higher levels in the experimental conditions than in the negative control (Fig. 4D and table S2).

To further filter these interacting proteins, we employed the RBP2GO score of the RBP2GO database (*47*) as a measure to identify strong RNA-binding proteins among these hits (Fig. 4E). We selected five of the top 10 proteins differentially bound to WT or NSExt *VHL* mRNA for validation of their effects on start site selection. The selected proteins that were preferentially bound to WT *VHL* mRNA included serine and arginine rich splicing factor 6 (SRSF6), eukaryotic translation initiation factor 4A1 (EIF4A1), ribosomal protein S3 (RPS3), poly-A binding protein cytoplasmic 1 (PABPC1), and ribosomal protein SA (RPSA). The selected genes that preferentially bound to the NSExt *VHL* mRNA were serine and arginine rich splicing factor 7 (SRSF7), ribosomal protein L23A (RPL23A), nucleolar protein 2 (NOP2), U3 small nucleolar ribonucleoprotein (IMP3), and far upstream element binding protein 1 (FUBP1). We additionally selected two eukaryotic translation initiation factors, EIF3D and EIF4G2, that had previously been linked to near-cognate start site selection (*48*). We screened these 12 genes using siPOOLs for their efficient and specific knockdown and evaluated their effects on VHL isoform distributions (fig. S8, A to E). The amount of VHL^{213}/VHL^{160} showed a significant increase, i.e., an increased selection of the first start site on NSExt *VHL* mRNA, upon knockdown of EIF4A1, EIF3D, and RPS3, while a nonsignificant increase was also seen with EIF4G2, SRSF6, PABPC1 and RPL23A (fig. S8F). A STRING (Protein-Protein Interaction Networks Functional Enrichment Analysis) network analysis of the aforementioned 12 proteins uncovered that they mainly belong to three different complexes and functions—translation initiation, ribosome, and splicing (fig. S9A). Thus, we further validated the top regulatory genes from these complexes in *VHL* NSExt cells and confirmed that the translation initiation factors EIF4A1, EIF3D, and EIF4G2 and the poly-A binding protein PABPC1 played an important role in regulating the start site selection in *VHL* NSExt cells (Fig. 4, F and G). It was reaffirming to see the involvement of initiation complex factors in the start site selection process. To confirm that the impact of these factors on VHL start site selection was specific, we tested a broad panel of 13 additional translation factors by siPOOL-mediated knockdown. The knockdown of none of these known translation start codon selection factors, ribosome recycling factors, translation termination factors, and stop codon-binding initiation factors (*49*–*54*) showed any significant increase in earlier start site selection (fig. S9, B to E). In conclusion, specifically the translation initiation factors EIF4A1, EIF3D, EIF4G2, and poly-A binding protein PABPC1 differentially regulated the start site selection in the *VHL* NSExt genotype.

Germline *VHL* nonstop mutations associate with severe disease phenotypes in a patient cohort

Patients with VHL syndrome develop various types of tumors in their lifetime, particularly ccRCCs, pheochromocytomas, or CNS tumors. Usually, these patients inherit a germline mutation of the VHL gene from an affected parent and a WT gene from the unaffected parent. In affected individuals, the germline mutation is present in all cell types (first hit); however, tumor formation occurs only in cell types with somatic inactivation of the normal allele (second hit) (*55*). So far, mostly deletions, missense, and nonsense mutations have been studied as loss-of-function aberrations in the *VHL* gene. However, in the Freiburg VHL registry, we found four patients with germline nonstop mutations in *VHL* (Fig. 5A).

According to observational data, individuals with VHL syndrome develop tumors more frequently and at a younger age (*56*). For the *VHL* nonstop mutations, all patients developed a severe disease manifestation by the age of 40 years with a disease penetrance of 100%, with one patient developing disease as early as with 15 years of age (Fig. 5B). The disease penetrance and the early onset of disease of the *VHL* nonstop Ter214Gly (*>G) mutation was comparable with that of the known pathogenic Arg167Trp mutation carriers (Fig. 5B). Magnetic resonance imaging revealed the VHL disease penetrance of patients with the nonstop mutant *VHL* by the diagnosis of ccRCC (Fig. 5C) or pheochromocytoma (Fig. 5D) as well as retinal angioma, CNS hemangioblastoma, or pancreatic neuroendocrine tumor, conclusively documenting the clinical relevance of *VHL* nonstop mutations.

The importance of germline *VHL* nonstop mutation was further validated by additional case reports of patients developing VHL syndrome-linked tumors (*57*, *58*) including a case of the *>L nonstop mutation and another stop codon change, *>R, that was recently reported in a Korean population (*58*). To further validate the importance of these *VHL* nonstop germline mutations found in patients, we introduced the *>G and *>R mutations into the endogenous genomic VHL locus in HEK293 cells via precision genome editing and generated three independent homozygous clones per genotype (fig. S10, A to C). A strong loss of VHL protein expression with a concomitant increase in HIF-1α protein levels was observed

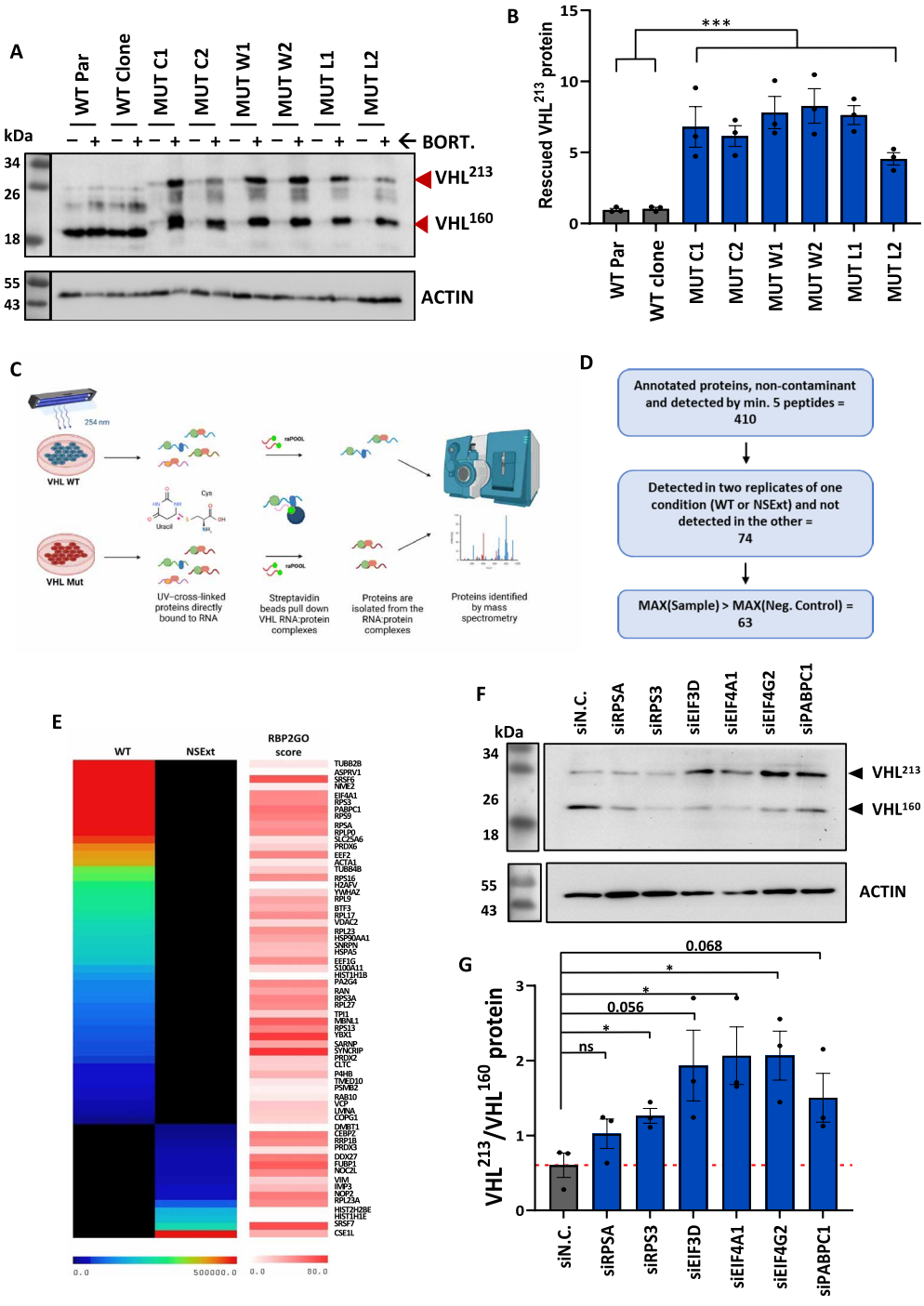

Fig. 4. Nonstop mutations in *VHL* alter translational start codon selection. (**A** and **B**) Bortezomib (Bort.) treatments of mutant cells resulted in an increased expression specifically of the larger isoform of VHL in mutants (MUT) compared to wild types (WT) [quantification in (B), $N = 3$]. VHL^{213} represents the 213–amino acid–long VHL isoform translated from the first translational start codon and VHL^{160} refers to the 160–amino acid–long VHL isoform translated from the second translational start codon. (**C**) Schematic workflow of RNA affinity purification followed by mass spectrometry (RAP-MS). Cells were UV–cross-linked to fix the RNA-bound proteins directly on the RNAs. *VHL* mRNAs were pulled down using an raPOOL of 30 different biotinylated probes binding to *VHL* compared to a non-targeting control raPOOL. *VHL*-bound proteins were identified using mass spectrometry. Created in BioRender. Pal (2024); https://BioRender.com/o16w486. (**D**) Schematic workflow of the data analysis steps to identify *VHL* mRNA-bound proteins from the RAP-MS differentially binding to *VHL* WT versus mutant mRNAs (NSExt and MUT C2). (**E**) Heatmap of the differentially bound proteins to *VHL* WT and NSExt mRNA from RAP-MS including their propensity to bind to RNA as indicated by the RBP2GO score ($N = 3$). (**F** and **G**) siPOOL-mediated knockdown of ribosomal proteins RPSA and RPS3; translation initiation factors EIF3D, EIF4A1, and EIF4G2; and the poly-A binding protein PABPC1 in *VHL* NSExt (MUT C2) cells altered the VHL protein isoform ratio with an increase in VHL^{213} abundance [quantification in (G) $N = 3$]. siN.C. refers to the non-targeting siPOOL control. For (B) and (G), *F* tests followed by unpaired *t* tests were performed. Here, ns, *, and *** refer to *P* values of >0.05, <0.05, and <0.001, respectively.

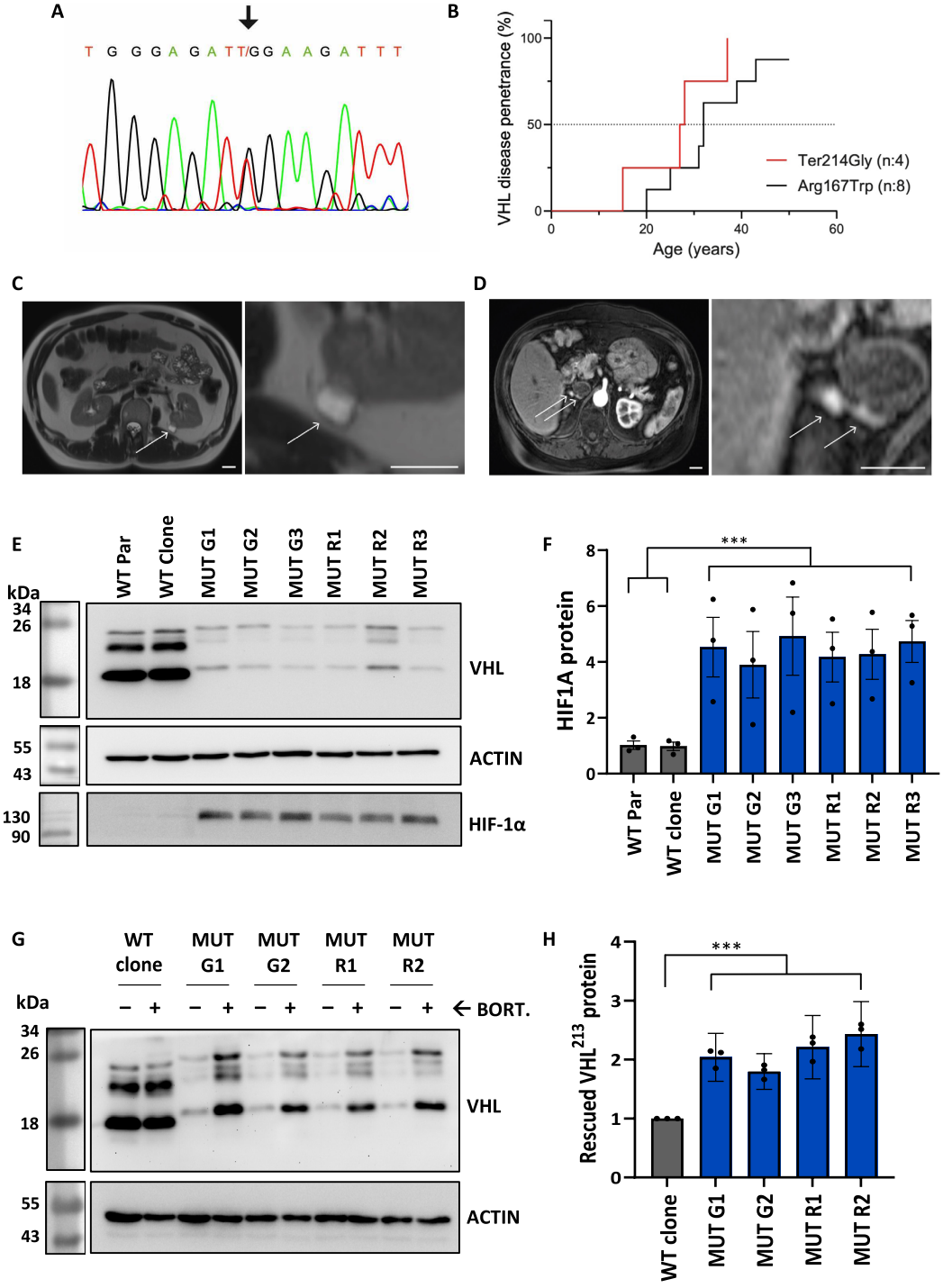

Fig. 5. Clinical implication of germline *VHL* nonstop mutations. (**A**) PCR-mediated sequencing of blood samples from an individual carrying the heterozygous germline nonstop variant *VHL* c.640T>G (p.Ter214Gly). (**B**) A Kaplan-Meier estimator assessing the age-related VHL disease penetrance (first diagnosis of retinal angioma, CNS hemangioblastoma, clear cell renal cell carcinoma, pancreatic neuroendocrine tumor, or pheochromocytoma) in participants of the Freiburg VHL Registry carrying the *VHL* nonstop variant c.640T>G (p.Ter214Gly) in comparison to the disease penetrance of carriers of the pathogenic variant c.499C>T (p.Arg167Trp), which revealed no significant difference (log-rank test). (**C** and **D**) Magnetic resonance images displaying clear cell renal cell carcinoma (C, right panel: 5× magnification) and pheochromocytoma (D, right panel: 5× magnification) in carriers of *VHL* nonstop variants. Scale bars represent 20 mm. (**E** and **F**) *VHL* *>G and *>R nonstop mutations also led to protein loss and HIF-1α stabilization [quantification in (F), $N = 3$]. *>G and *>R refer to the stop codon change to Gly and Arg, respectively. The numbers identify the different homozygous clones for each genotype to exclude clone-specific differences. (**G** and **H**) The mutant protein expression was rescued by bortezomib (BORT.) treatment. Also, the VHL^{213} isoform was significantly more stabilized for the mutant *VHL* compared to WT [quantification in (H), $N = 3$]. For (F) and (H), an *F* test followed by an unpaired *t* test was performed where *** refers to a *P* value of <0.001.

in the NSExt mutant cells (Fig. 5, E and F). In addition, the NSExt VHL protein was rescued by the treatment of the cells with bortezomib, suggesting its degradation via the ubiquitin-proteasome pathway. A selective increase in VHL^{213} levels in the mutants also showed altered start site selection in nonstop mutant *VHL* cell lines (Fig. 5, G and H) comparable to the results obtained for the somatic *>C, *>W, and *>L *VHL* nonstop mutations.

In conclusion, we reported additional germline nonstop mutations in *VHL* that caused substantial protein loss and disease phenotypes with early onset and high penetrance in patients with VHL syndrome highlighting the importance of nonstop mutations in *VHL* in disease development and progression.

Taken together, this study uncovered that nonstop mutations caused a strong reduction of the kidney tumor suppressor proteins VHL and BAP1. This protein loss was mediated via different mechanisms, i.e., translation inhibition for BAP1 and proteasomal degradation for VHL plus alternative translational start site selection for VHL, thus affecting translation at multiple levels.

DISCUSSION

The functional effect of nonstop extensions mutations in cancer remains largely unexplored. The NonStopDB brought to light 3412 nonstop mutations in a pan-cancer analysis based on the COSMIC database (*18*). Nonstop mutations in the *SMAD4* tumor suppressor gene led to loss of the protein and increased tumorigenic phenotypes predominantly and specifically in pancreatic and colon cancer (*18*). Further nonstop mutations in *SMAD4* were recently reported in four patients (two pancreatic adenocarcinomas, one colonic adenocarcinoma, and one non–small cell lung carcinoma) with a loss of the protein as confirmed by immunohistochemistry (*59*). A meta-analysis of the Human Gene Mutation Database (HGMD) revealed 119 nonstop mutations in 87 different genes known to cause human inherited diseases (*6*) further highlighting the potential impact of nonstop mutations in disease progression. In conclusion, these non-canonical mutations in cancer need to be studied further for their impact on tumorigenesis, progression, and therapy response—as they can have similarly strong effects as the better-studied missense or nonsense mutations. This will aid in tailoring personalized therapies, revealing mechanisms of gene regulation and informing strategies for hereditary cancer syndromes.

In the present study, we hypothesized that additional cancer genes that were both recurrently affected by nonstop mutations and were frequently altered by other forms of point mutations could have pathogenic consequences in tumors. Rare mutations that were driver mutations were often tissue specific (*60*). Our analyses revealed *VHL* and *BAP1* tumor suppressor genes to be recurrently altered by nonstop mutations in a tumor-specific manner, i.e., enriched in patients with kidney cancer. Comprehensive characterization of the mutation spectrum from TCGA revealed that *VHL* (first) and *BAP1* (fifth) were among the top driver genes involved in kidney cancer pathogenesis (*30*). In addition, mutations altering the stop codon of *BAP1* or *VHL* in cancer were also found in other databases (*61*).

Stop-loss or nonstop mutations in *BAP1* led to a 205–amino acid–long extension in the C terminus, resulting in the loss of the BAP1 protein and an increase in histone H2A-K119 ubiquitination levels, a direct substrate of the deubiquitinase BAP1 (*62*). The loss in BAP1 protein was linked to neither decreased mRNA levels nor protein degradation. In addition, translation of a second downstream ORF in the *BAP1* 3'UTR (predicted protein HUCEP13), which could have had an influence on the expression of the upstream BAP1 ORF (*36*), did not affect NSExt BAP1 protein expression. However, in vitro transcription-translation assays showed a reduction in the translation of the NSExt mRNAs. Adding to this observation, polysome fractionation coupled with reverse transcription quantitative polymerase chain reaction (RT-qPCR) quantification revealed a significant reduction of the BAP1 NSExt mRNAs in the heavy polysome fraction. A similar observation of reduced translation had been made for a synthetic gene with green fluorescent protein lacking any stop codon in a "readthrough" scenario (*63*). The depletion of the NSExt *BAP1* mRNA from the heavy polysome fraction could be due to lower efficiency of either translation initiation or elongation and ribosome stalling as observed for readthrough mRNAs (*63*).

NSExt mutations in *VHL* created a 14–amino acid extension with increased hydrophobicity at its C terminus leading to rapid degradation by the ubiquitin-proteasome pathway. This is in accordance with previous findings in the *SMAD4* tumor suppressor gene that harbors a hydrophobic degron in its C-terminal extension (*18*), as well as with the more general finding that translation into the 3'UTR could often result in decreased protein expression (*3*), and extensions enriched in hydrophobic residues are consequently degraded by the proteasomal machinery (*43*).

Inactivation of *VHL* by missense mutations, deletions, or epigenetic silencing leads to different cancer types, particularly ccRCCs (*64*, *65*) where >90% of ccRCCs show somatic or germline VHL inactivation (*66*, *67*). VHL, an E3 ubiquitin ligase, targets and degrades the HIF1A transcription factor in hypoxic conditions (*31*). Our study showed that NSExt-mediated loss of the VHL protein led to increased HIF1A levels and its downstream transcriptional targets. In addition, the mutations increased the migration capacity (*68*). These findings thus also showed the loss of VHL function at the molecular and cellular level.

Patients with germline *VHL* inactivating mutations have VHL syndrome, which is characterized by increased chances of inactivation of the second *VHL* allele and subsequent development of multiple tumors (*32*). In addition to the somatic mutations found in cancer listed in the NonStopDB (*18*), the repercussions of *VHL* NSExt mutations were corroborated by the additional four patients with germline *>G from the Freiburg VHL registry and two patients with germline *>L (*57*) and germline *>R (*58*) mutations all suffering from VHL syndrome with early onset and high penetrance of tumor development.

Nonstop readthrough mutations, i.e., nonstop mutations without a second in-frame stop codon, can cause mRNA degradation via the no-stop-decay (*1*, *2*) or inhibit translation of the protein (*63*). For BAP1, we also found an inhibition of translation caused by an NSExt mutation. For VHL, we discovered another impact of its NSExt mutations at the translational level: the alteration of translational start site selection and thus changes in the amounts of protein isoforms. Upon stabilization of the NSExt VHL protein by ubiquitin proteasome inhibitors, we observed a shift in the amount of the VHL^{213} versus the VHL^{160} isoforms; i.e., the longer VHL isoform derived from the first translational start site was increased in NSExt compared to WT cells. Several factors are known to determine start codon selection, such as RNA structure, relative accessibility of the AUG codon, length and nucleotide composition of the 5'UTR, and RNA-binding protein factors (*69*). RNA affinity purification followed by mass spectrometry (RAP-MS) determined differential

RNA-binding proteins on WT versus NSExt *VHL* mRNA. Validation experiments showed that the translation initiation factors EIF4A1, EIF3D, and EIF4G2 and the poly-A binding protein PABPC1 played a role in regulating the NSExt VHL start site selection. Knockdown of these proteins increased the amount of VHL^{213}, which implied that these factors promoted VHL^{160} translation. The RNA helicase EIF4A1 is important for pre-initiation complex (PIC) fidelity and preferential selection of 5′ start codons (*70*). EIF4G forms the scaffold of the PIC and interacts with PABPC1 and EIF4A1 to recruit the PIC to the start codon (*71*), while PABPC1 itself also controls translation initiation by interacting with the 5'UTR (*72*). From RAP-MS, EIF4A1 and PABPC1 were preferentially bound to the WT *VHL* mRNA. Their weaker interaction with the NSExt *VHL* mRNA may thus lead to the preferential production of VHL^{213} from NSExt *VHL* mRNA and additionally sensitize it to their further knockdown by siPOOLs leading to the even higher VHL^{213} to VHL^{160} ratio in the NSExt cells upon their knockdown. EIF4G2 and EIF3D interact with one another (*71*), regulate alternative or noncognate start codon selection (*48*), and bind to posttermination ribosomes (*73*). It is well established that there is a communication between translation initiation and termination through initiation factors and poly-A binding proteins whose interaction leads to the circularization of the mRNA during translation and bringing the termination and initiation sites into proximity (*74*). In line with this, we propose that the established complex of all four aforementioned proteins promotes interaction or cross-talk between translation start and termination and that their stoichiometry regulates VHL start codon selection, which, in turn, would give rise to different VHL isoforms (*75*).

In summary, we identified the kidney tumor suppressor genes *VHL* and *BAP1* to harbor recurrent somatic NSExt mutations. For both genes, the nonstop mutations led to a strong loss of the protein, but via different mechanisms: While the VHL NSExt protein was proteasomally degraded, the translation of the BAP1 protein was decreased and its expression could not be rescued by proteasome inhibition. Further, *VHL* NSExt mutations also resulted in altered translational start codon selection (fig. S10D). Thus, these results revealed additional mechanisms by which nonstop mutations can regulate protein expression at multiple stages of translation. The importance of understanding nonstop mutations was further highlighted by the discovery of germline *VHL* nonstop mutations leading to VHL-related diseases with high penetrance and early onset.

MATERIALS AND METHODS

Cell culture

The WT and NSExt mutant HEK293 cell lines were cultured in Iscove's modified Dulbecco's medium (IMDM) (Thermo Fisher Scientific Gibco, catalog number 21980065) supplemented with 10% fetal bovine serum (Thermo Fisher Scientific #10270106) at 37°C and 5% CO_2 in a humidified incubator. The parental HEK293 cells were a gift from the laboratory of T. Cathomen, University of Freiburg. The cells were fingerprinted using the Multiplex Cell Authentication service (Multiplexion) to check authenticity and were regularly tested negative for mycoplasma.

CRISPR-Cas–mediated precision genome editing and clone selection

The guide RNAs (gRNAs) were designed as per IDT's protocol for the stop codon mutations for *VHL* and *BAP1*. The gRNAs and the single-stranded oligodeoxynucleotides (ssODNs) were obtained from IDT and Synthego and their sequences are provided in table S3. Freshly thawed and split HEK293 cells were nucleofected according to IDT's protocol. For the nucleofection mix for the CRISPR-Cas12 method (for *VHL*), 5 μl of ribonucleoprotein (RNP) mix was formulated by mixing 1.6 μl of 100 μM Alt-R CRISPR-Cas12a crRNA (dissolved in IDTE Buffer; #11-01-02-02), 1.4 μl of 1× phosphate-buffered saline (PBS), and 2 μl of Alt-R A.s. Cas12a (Cpf1) Ultra (#10001272) in an Eppendorf tube and incubated for 20 min. Meanwhile, HEK293 cells were trypsinized, resuspended in media, and counted. A total of 100,000 cells were aliquoted in a tube, spun down at 100*g*, washed with 1× PBS, and pelleted down again at 100*g*. The cells were then resuspended in 20 μl of SF Cell Line buffer (SF Cell Line 4D-NucleofectorTM X Kit S, #V4XC-2032). One microliter of 78 μM Alt-R Cpf1 Electroporation Enhancer (IDT #1076300) and 1 μl of 100 μM ssODN (dissolved in water) were added to the cell mix and the total 22-μl cell suspension was mixed gently and added to the tube containing 5 μl of RNP mix. The resulting 27 μl of cell/RNP solution was mixed gently, added to 1 well of the 16-well Nucleocuvette Strip and immediately electroporated with the DS-150 protocol in the 4D-Nucleofector System (Lonza #AAF-1002B with AAF-1002X).

For the nucleofection mix for the CRISPR-Cas9 method (for *BAP1*), 2.8 μl of RNP mix was formulated by mixing 1.8 μl of 100 μM Synthego Synthetic sgRNA (dissolved in 10 mM tris and 1 mM EDTA, pH 8.0) and 1 μl of *Staphylococcus pyogenes* Cas9 enzyme (NEB #M0386M) in an Eppendorf tube and incubated for 20 min. Meanwhile, HEK293 cells were trypsinized, resuspended in media, and counted. A total of 100,000 cells were aliquoted in a tube, spun down at 100*g*, washed with 1× PBS, and pelleted down again at 100*g*. The cells were then resuspended in 20 μl of SF Cell Line buffer (SF Cell Line 4D-NucleofectorTM X Kit S, #V4XC-2032). One microliter of 100 μM ssODN (dissolved in water) was added to the cell mix and the total 21 μl of cell suspension was mixed gently and added to the tube containing 2.8 μl of RNP mix. The resulting 23.8 μl of cell/RNP solution was mixed gently, added to 1 well of the 16-well Nucleocuvette Strip and immediately electroporated with the CM-130 protocol in the 4D-Nucleofector System (Lonza #AAF-1002B with AAF-1002X).

For both methods, after the nucleofection, the cells were incubated at room temperature for 10 min and subsequently transferred to a 12-well dish containing 1 ml of media containing 1 μM Alt-R HDR Enhancer V2 (#10007910) and incubated at 37°C with 5% CO_2.

The cells were harvested after approximately 1 week when they were ~80% confluent. The cells were counted and plated in a dilution of 0.5 cells per well in six 96-well plates for the isolation of clones. The remaining cells were pelleted down and used for genomic DNA isolation to test the percentage of mutation at the locus of interest using Sanger sequencing. The single cell clones were sequenced subsequently to pick the positive clones (fig. S1, B and C). The number of clones sequenced was dependent on the percentage of mutated peak in the bulk cell sequencing.

Western blotting

Cells were harvested by trypsinization and pelleted at 100*g*. The cells were then lysed using RIPA lysis buffer (50 mM tris, pH 8.0, 150 mM NaCl, 0.5% sodium deoxycholate, 0.1% SDS, and 1% NP-40) containing 1× phosphatase inhibitor (PhosSTOP, Roche #4906837001) and 1× protease inhibitor cocktails (cOmplete EDTA-free, Roche #4693132001) on ice for 1 hour. The lysates were centrifuged at

17,000*g* for 30 min at 4°C. The protein concentration was quantified using Bradford reagent and a standard bovine serum albumin (BSA) curve. Protein (5 to 15 μg) was mixed with 6× Laemmli buffer (0.25 M tris, pH 6.8, 20% glycerol, 10% 2-mercaptoethanol, 0.002% bromophenol blue, and 4% SDS). In some instances, cells were also lysed directly by adding the 2× SDS loading/sample buffer [100 mM tris-Cl, pH 6.8, 4% SDS, 0.2% bromophenol blue, 20% glycerol, and 200 mM dithiothreitol (DTT)]. All samples were heated at 95°C for 10 min and separated on 10 to 12.5% SDS–polyacrylamide gel electrophoresis (SDS-PAGE) gels. The proteins were transferred using semidry transfer buffer (48 mM tris, 39 mM glycine, and 20% methanol) onto polyvinylidene fluoride (PVDF) membrane at 10 V for 60 min. Next, the membrane was blocked in 5% milk in 1× TBST (20 mM tris-Cl, pH 7.6, 158 mM NaCl, and 0.1% Tween-20) for 1 hour. The primary antibodies were diluted in 5% BSA or milk in 1× TBST and used for overnight incubation at 4°C. The blots were washed 3× in TBST and incubated in horseradish peroxidase–conjugated anti-rabbit or anti-mouse secondary antibody for 1 hour at room temperature. Last, the membranes were washed 3× with TBST for 10 min and developed using SuperSignal West Pico Chemiluminescent Substrate (Thermo Fisher Scientific #43078) or ECL Prime Western Detection Reagent (VWR/Amersham #RPN2232). Images were acquired on a ChemoCam Imager, bands were quantified using ImageJ software (*76*), and positive background was subtracted from the signal density. The molecular weight in kilodaltons according to the marker is given next to each blot. All uncropped blots are provided as source data files. The list of antibodies is provided in table S3.

Polysome fractionation

The cells were grown in 60-mm dishes to 90% confluency. CHX (100 μg/ml final concentration; Sigma-Aldrich #66-81-9) was added to the same media just 3 min before harvesting. After CHX treatment for 3 min, all the media was removed and the cells were washed two times with 3 ml of PBS containing CHX (100 μg/ml). Depending on the cell density, 300 to 500 μl of lysis buffer [20 mM tris, pH 7.4, 1.5 mM KCl, 5 mM $MgCl_2$, 1 mM DTT, CHX (100 μg/ml), 0.1 mM sodium deoxycholate, 0.5% Triton X-100, protease inhibitor (VWR #PAG6521), and RNase inhibitor (Promega #N2511)] was added to each dish and cells were scraped and collected into tubes. The tubes were rotated in lysis buffer for 15 min at 4°C. The KCl concentration in the buffer was adjusted to 150 mM by adding 3 M KCl. The cell debris were pelleted at 10,000*g* for 10 min and the clear lysate was transferred into fresh RNA-free tubes.

Sucrose solutions (5 and 50%) were prepared in polysome buffer [20 mM tris, pH 7.4, 150 mM KCl, 5 mM $MgCl_2$, 1 mM DTT, and CHX (100 μg/ml)]. Approximately 10 ml of each solution was loaded onto TH641 tubes and the gradient was created using a gradient master. The Optical Density (O.D.) of the lysates was measured and 200 μg of RNA-containing lysate was loaded on top of the gradient. The tubes were then centrifuged at 36,000 rpm for 2 hours using a TH641 rotor (Sorvall). After centrifugation, the gradients were analyzed at an absorbance of 260 nm using a BIOCOMP fraction analyzer and the fractions were collected. RNA was isolated from the fractions using the Quick-RNA Microprep Kit (Zymo Research #R1051), subjected to cDNA conversion, and the genes were measured by RT-qPCR.

Protein stability assay

To assess the stability of WT versus NSExt mutant VHL, CHX (Sigma-Aldrich #66-81-9) chase experiments were performed. First, the WT and NSExt mutant cell lines were treated with 0.1 μM bortezomib to stabilize and detect the mutant protein by Western blot for the chase. After 8 hours, the bortezomib-containing media was removed, cells were washed 3× with fresh media, and then CHX (100 μg/ml) was added. The cells were harvested at 0-, 6-, 12-, 24-, and 36-hour time points, resuspended in 2× SDS sample buffer, boiled at 95°C for 10 min, snap chilled on ice, and loaded for Western blot analysis.

RNA affinity purification

The RNA affinity pool (raPOOL) probes targeting the coding sequence of *VHL* (20 bp away from the stop codon) were designed and ordered from siTOOLs Biotech, Martinsried (sequences provided in table S3). These raPOOLs consist of 30 single-stranded 3′-biotinylated DNA oligonucleotides (20 bases length) and hybridize to the entire length of the target RNA sequence. raPOOLs that hybridize to the bacterial LacZ RNA were used as negative control.

Cells were grown to a density of ~90% in 15-cm dishes. The cells were washed one time with 1× PBS. Five milliliters of ice-cold 1× PBS was added to each plate and the cells were then subjected to UV–cross-linking on ice using a Stratagene Stratalinker 2400 UV Cross-linker. The cells were then scraped and resuspended in 1× PBS. Cells were counted and 20 million cells were aliquoted into 50-ml falcons. The cells were pelleted at 2000*g* for 5 min at 4°C, resuspended in 1 ml of ice-cold 1× PBS, transferred into fresh 2-ml Eppendorf tubes, and again centrifuged at 2000*g* for 3 min at 4°C. All of the PBS was carefully removed, and the pellets were snap frozen in liquid nitrogen and stored at −80°C. The next day, the pellets were resuspended in 500 μl of ice-cold lysis buffer (50 mM tris-Cl, pH 7.0, 10 mM EDTA, and 1% SDS, with protease and nuclease inhibitors added fresh before use). The samples were loaded in 1-ml Covaris tubes (Covaris milliTUBE 1 ml AFA Fiber, #520135) and sonicated in a Covaris M220 focused sonicator to get 200- to 500-bp fragments making sure that the tubes remained below 10°C. Dynabeads MyOne Streptavidin C1 (600 μl; Thermo Fisher Scientific #65001) was washed 3× with lysis buffer and lastly resuspended in 600 μl of lysis buffer. To the fragmented samples in lysis buffer, 1 ml of hybridization buffer (750 mM NaCl, 1% SDS, 50 mM tris-Cl, pH 7.0, 1 mM EDTA, and 15% formamide, with protease and nuclease inhibitors added fresh before use) was added and gently mixed. The lysates were precleared by adding 30 μl of the beads, incubating at 37°C for 30 min with gentle rocking and removing the beads by using a magnetic stand. The raPOOLs were then added to each sample at a final concentration of 100 pmol per 20 million cells. Hybridization was carried out for 4 hours at 37°C with agitation. Next, 100 μl of the washed beads was added to each sample and incubated at 37°C for 30 min with agitation. The beads were collected using a magnetic stand. Next, the beads containing the RNA-protein complexes were washed five times in 1 ml of 37°C prewarmed wash buffer (2× sodium chloride, sodium citrate, and 0.5% SDS, with protease and nuclease inhibitors added fresh before use). During each wash, the tubes were agitated for 5 min at 37°C and then the beads were collected with a magnetic stand.

At the final step, the beads were magnetically separated from the wash buffer and resuspended in 1 ml of benzonase elution buffer [20 mM tris, pH 8.0, 0.05% *N*-lauroylsarcosine, 2 mM $MgCl_2$, and 0.5 mM tris (2-carboxyethyl)phosphine]. Benzonase nonspecific nuclease (125 U; Sigma-Aldrich #E1014) was added and incubated for 2 hours at 37°C, agitating at 1100 rpm, 1 min on and 10 min off. The beads were magnetically separated from the eluate, and this was repeated 5× until all beads were eliminated. The proteins were then

precipitated with trichloroacetic acid at a final concentration of 10%. The samples were incubated with gentle rocking at 4°C overnight and subsequently centrifuged at 16,000 rpm for 3 min. The supernatant was discarded and replaced with 1 ml of cold acetone and then centrifuged again at 16,000 rpm for 15 min at 4°C. The pellets were then air dried, snap frozen in liquid nitrogen, and stored at −80°C for further processing for mass spectrometry.

siPOOL transfection

For knockdown of the target genes using siPOOLs, cells were reverse transfected with 10 nM (final concentration) of nontargeting control (siN.C.) or siPOOL of all targets (siTOOLs Biotech) using Lipofectamine RNAiMAX (2 µl per well; Invitrogen, Waltham MA, USA) in 12-well plates (0.35×10^6 cells per well). Cells were collected after 48 hours for protein lysis and Western blotting. For experiments requiring siPOOL transfection followed by bortezomib treatment, bortezomib was added directly to a final concentration of 0.1 µM without changing the media after 24 hours of siPOOL reverse transfection. siPOOL sequences are provided in table S3.

Freiburg VHL registry, study design, and participants

The Freiburg VHL Registry includes patients who were screened at least once at the von Hippel-Lindau Outpatient Clinic of the University Medical Center Freiburg until 1 March 2024. Inclusion criteria for this retrospective analysis were the detection of a *VHL* germline mutation by Sanger sequencing for intra-exonic variants, by multiplex ligation-dependent probe amplification analysis for large deletions and rearrangements, or by next-generation sequencing–based multigene panels. Patients without clinical data were excluded. Clinical surveillance was performed according to international guidelines for VHL disease (VHL Active Surveillance Guidelines) and included ophthalmoscopy with complete peripheral retinal examination, radiologic imaging with contrast-enhanced magnetic resonance imaging (MRI) of the brain and spinal cord, and MRI of the abdomen. Clinical data such as age, sex, and diagnostic findings were recorded in a predefined database. The time of the first ophthalmologic diagnosis of retinal angioma or the first radiologic description of CNS hemangioblastoma, ccRCC, pancreatic neuroendocrine tumor, or pheochromocytoma was considered the first manifestation of VHL disease. The use of anonymized data for further analysis was approved by the Ethics Committee of the University of Freiburg (EK-FR 79/2).

Data representation, normalization, and statistical analyses

All experiments were performed in three independent biological replicates unless otherwise mentioned. All RT-qPCR experiments (except Fig. 2, E and F, and fig. S3H) were normalized to the internal control gene *cyclophilin A* mRNA (*PPIA*). For the polysome fractionation (Fig. 2, E and F), the RNA levels were normalized to the amounts in the free RNA fraction. For the in vitro transcription/translation (fig. S3H), *BAP1* mRNA was normalized to 28S rRNA from the rabbit reticulocyte lysate. All Western blot quantifications were normalized to the actin loading controls. The individual values were further normalized to the average of the WTs, the latter being normalized to 1. All graphs were generated using GraphPad Prism version 10.0.2. The SEM was represented in the graphs. For box plots, the mean, minimum, and maximum values were represented. For statistical comparisons, unpaired *t* tests after *F* tests for heteroscedasticity were used. *, **, and *** refer to *P* values of <0.05, <0.01, and <0.001, respectively. "ns" represents nonsignificant.

Supplementary Materials

The PDF file includes:

Supplementary Methods
Legends for tables S1 to S3
Legends for data S1 and S2
Figs. S1 to S10

Other Supplementary Material for this manuscript includes the following:

Tables S1 to S3
Data S1 and S2

REFERENCES AND NOTES

1. A. A. Klauer, A. van Hoof, Degradation of mRNAs that lack a stop codon: A decade of nonstop progress. *Wiley Interdiscip. Rev. RNA* **3**, 649–660 (2012).
2. P. A. Frischmeyer, A. van Hoof, K. O'Donnell, A. L. Guerrerio, R. Parker, H. C. Dietz, An mRNA surveillance mechanism that eliminates transcripts lacking termination codons. *Science* **295**, 2258–2261 (2002).
3. J. A. Arribere, E. S. Cenik, N. Jain, G. T. Hess, C. H. Lee, M. C. Bassik, A. Z. Fire, Translation readthrough mitigation. *Nature* **534**, 719–723 (2016).
4. M. M. Yordanova, G. Loughran, A. V. Zhdanov, M. Mariotti, S. J. Kiniry, P. B. F. O'Connor, D. E. Andreev, I. Tzani, P. Saffert, A. M. Michel, V. N. Gladyshev, D. B. Papkovsky, J. F. Atkins, P. V. Baranov, AMD1 mRNA employs ribosome stalling as a mechanism for molecular memory formation. *Nature* **553**, 356–360 (2018).
5. N. Shibata, N. Ohoka, Y. Sugaki, C. Onodera, M. Inoue, Y. Sakuraba, D. Takakura, N. Hashii, N. Kawasaki, Y. Gondo, M. Naito, Degradation of stop codon read-through mutant proteins via the ubiquitin-proteasome system causes hereditary disorders. *J. Biol. Chem.* **290**, 28428–28437 (2015).
6. S. E. Hamby, N. S. T. Thomas, D. N. Cooper, N. Chuzhanova, A meta-analysis of single base-pair substitutions in translational termination codons ('nonstop' mutations) that cause human inherited disease. *Hum. Genomics* **5**, 241–264 (2011).
7. R. Vidal, B. Frangione, A. Rostagno, S. Mead, T. Révész, G. Plant, J. Ghiso, A stop-codon mutation in the BRI gene associated with familial British dementia. *Nature* **399**, 776–781 (1999).
8. O. M. El-Agnaf, J. M. Sheridan, C. Sidera, G. Siligardi, R. Hussain, P. I. Haris, B. M. Austen, Effect of the disulfide bridge and the C-terminal extension on the oligomerization of the amyloid peptide ABri implicated in familial British dementia. *Biochemistry* **40**, 3449–3457 (2001).
9. J. Sun, Z. Hao, H. Luo, C. He, L. Mei, Y. Liu, X. Wang, Z. Niu, H. Chen, J.-D. Li, Y. Feng, Functional analysis of a nonstop mutation in MITF gene identified in a patient with Waardenburg syndrome type 2. *J. Hum. Genet.* **62**, 703–709 (2017).
10. A. S. Bock, S. Günther, J. Mohr, L. V. Goldberg, A. Jahic, C. Klisch, C. A. Hübner, S. Biskup, C. Beetz, A nonstop variant in REEP1 causes peripheral neuropathy by unmasking a 3'UTR-encoded, aggregation-inducing motif. *Hum. Mutat.* **39**, 193–196 (2018).
11. J. Torres-Torronteras, A. Rodriguez-Palmero, T. Pinós, A. Accarino, A. L. Andreu, G. Pintos-Morell, R. Martíí, A novel nonstop mutation in *TYMP* does not induce nonstop mRNA decay in a MNGIE patient with severe neuropathy. *Hum. Mutat.* **32**, E2061–E2068 (2011).
12. S. Pang, W. Wang, B. Rich, R. David, Y. T. Chang, G. Carbunaru, S. E. Myers, A. F. Howie, K. J. Smillie, J. I. Mason, A novel nonstop mutation in the stop codon and a novel missense mutation in the type II 3β-hydroxysteroid dehydrogenase (3β-HSD) gene causing, respectively, nonclassic and classic 3β-HSD deficiency congenital adrenal hyperplasia. *J. Clin. Endocrinol. Metab.* **87**, 2556–2563 (2002).
13. S. Diederichs, L. Bartsch, J. C. Berkmann, K. Fröse, J. Heitmann, C. Hoppe, D. Iggena, D. Jazmati, P. Karschnia, M. Linsenmeier, T. Maulhardt, L. Möhrmann, J. Morstein, S. V. Paffenholz, P. Röpenack, T. Rückert, L. Sandig, M. Schell, A. Steinmann, G. Voss, J. Wasmuth, M. E. Weinberger, R. Wullenkord, The dark matter of the cancer genome: Aberrations in regulatory elements, untranslated regions, splice sites, non-coding RNA and synonymous mutations. *EMBO Mol. Med.* **8**, 442–457 (2016).
14. C. Kandoth, M. D. McLellan, F. Vandin, K. Ye, B. Niu, C. Lu, M. Xie, Q. Zhang, J. F. McMichael, M. A. Wyczalkowski, M. D. M. Leiserson, C. A. Miller, J. S. Welch, M. J. Walter, M. C. Wendl, T. J. Ley, R. K. Wilson, B. J. Raphael, L. Ding, Mutational landscape and significance across 12 major cancer types. *Nature* **502**, 333–339 (2013).
15. B. Zirn, S. Wittmann, M. Gessler, Novel familial WT1 read-through mutation associated with Wilms tumor and slow progressive nephropathy. *Am. J. Kidney Dis.* **45**, 1100–1104 (2005).
16. M. H. Bailey, C. Tokheim, E. Porta-Pardo, S. Sengupta, D. Bertrand, A. Weerasinghe, A. Colaprico, M. C. Wendl, J. Kim, B. Reardon, P. K.-S. Ng, K. J. Jeong, S. Cao, Z. Wang, J. Gao,

Q. Gao, F. Wang, E. M. Liu, L. Mularoni, C. Rubio-Perez, N. Nagarajan, I. Cortés-Ciriano, D. C. Zhou, W.-W. Liang, J. M. Hess, V. D. Yellapantula, D. Tamborero, A. Gonzalez-Perez, C. Suphavilai, J. Y. Ko, E. Khurana, P. J. Park, E. M. Van Allen, H. Liang, MC3 Working Group, Cancer Genome Atlas Research Network, M. S. Lawrence, A. Godzik, N. Lopez-Bigas, J. Stuart, D. Wheeler, G. Getz, K. Chen, A. J. Lazar, G. B. Mills, R. Karchin, L. Ding, Comprehensive characterization of cancer driver genes and mutations. *Cell* **173**, 371–385.e18 (2018).

17. M. Sinkala, Mutational landscape of cancer-driver genes across human cancers. *Sci. Rep.* **13**, 12742 (2023).
18. S. Dhamija, C. M. Yang, J. Seiler, K. Myacheva, M. Caudron-Herger, A. Wieland, M. Abdelkarim, Y. Sharma, M. Riester, M. Groß, J. Maurer, S. Diederichs, A pan-cancer analysis reveals nonstop extension mutations causing SMAD4 tumour suppressor degradation. *Nat. Cell Biol.* **22**, 999–1010 (2020).
19. K. De Bosscher, C. S. Hill, F. J. Nicolas, Molecular and functional consequences of Smad4 C-terminal missense mutations in colorectal tumour cells. *Biochem. J.* **379**, 209–216 (2004).
20. K. L. Woodford-Richens, A. J. Rowan, P. Gorman, S. Halford, D. C. Bicknell, H. S. Wasan, R. R. Roylance, W. F. Bodmer, I. P. M. Tomlinson, SMAD4 mutations in colorectal cancer probably occur before chromosomal instability, but after divergence of the microsatellite instability pathway. *Proc. Natl. Acad. Sci. U.S.A.* **98**, 9719–9723 (2001).
21. H. Alazzouzi, P. Alhopuro, R. Salovaara, H. Sammalkorpi, H. Järvinen, J.-P. Mecklin, A. Hemminki, S. Schwartz, L. A. Aaltonen, D. Arango, SMAD4 as a prognostic marker in colorectal cancer. *Clin. Cancer Res.* **11**, 2606–2611 (2005).
22. A. Ghosh, M. Riester, J. Pal, K.-A. Lainde, C. Tangermann, A. Wanninger, U. K. Dueren, S. Dhamija, S. Diederichs, Suppressive cancer nonstop extension mutations increase C-terminal hydrophobicity and disrupt evolutionarily conserved amino acid patterns. *Nat. Commun.* **15**, 9209 (2024).
23. NonStopDB; Database of Nonstop Mutations in Cancer. https://NonStopDB.dkfz.de.
24. Z. Sondka, N. B. Dhir, D. Carvalho-Silva, S. Jupe, Madhumita, K. M. Laren, M. Starkey, S. Ward, J. Wilding, M. Ahmed, J. Argasinska, D. Beare, M. S. Chawla, S. Duke, I. Fasanella, A. G. Neogi, S. Haller, B. Hetenyi, L. Hodges, A. Holmes, R. Lyne, T. Maurel, S. Nair, H. Pedro, A. Sangrador-Vegas, H. Schuilenburg, Z. Sheard, S. Y. Yong, J. Teague, COSMIC: A curated database of somatic variants and clinical data for cancer. *Nucleic Acids Res.* **52**, D1210–D1217 (2024).
25. Z. Sondka, S. Bamford, C. G. Cole, S. A. Ward, I. Dunham, S. A. Forbes, The COSMIC Cancer Gene Census: Describing genetic dysfunction across all human cancers. *Nat. Rev. Cancer* **18**, 696–705 (2018).
26. E. Cerami, J. Gao, U. Dogrusoz, B. E. Gross, S. O. Sumer, B. A. Aksoy, A. Jacobsen, C. J. Byrne, M. L. Heuer, E. Larsson, Y. Antipin, B. Reva, A. P. Goldberg, C. Sander, N. Schultz, The cBio cancer genomics portal: an open platform for exploring multidimensional cancer genomics data. *Cancer Discov.* **2**, 401–404 (2012).
27. A. Zehir, R. Benayed, R. H. Shah, A. Syed, S. Middha, H. R. Kim, P. Srinivasan, J. Gao, D. Chakravarty, S. M. Devlin, M. D. Hellmann, D. A. Barron, A. M. Schram, M. Hameed, S. Dogan, D. S. Ross, J. F. Hechtman, D. F. DeLair, J. Yao, D. L. Mandelker, D. T. Cheng, R. Chandramohan, A. S. Mohanty, R. N. Ptashkin, G. Jayakumaran, M. Prasad, M. H. Syed, A. B. Rema, Z. Y. Liu, K. Nafa, L. Borsu, J. Sadowska, J. Casanova, R. Bacares, I. J. Kiecka, A. Razumova, J. B. Son, L. Stewart, T. Baldi, K. A. Mullaney, H. Al-Ahmadie, E. Vakiani, A. A. Abeshouse, A. V. Penson, P. Jonsson, N. Camacho, M. T. Chang, H. H. Won, B. E. Gross, R. Kundra, Z. J. Heins, H.-W. Chen, S. Phillips, H. Zhang, J. Wang, A. Ochoa, J. Wills, M. Eubank, S. B. Thomas, S. M. Gardos, D. N. Reales, J. Galle, R. Durany, R. Cambria, W. Abida, A. Cercek, D. R. Feldman, M. M. Gounder, A. A. Hakimi, J. J. Harding, G. Iyer, Y. Y. Janjigian, E. J. Jordan, C. M. Kelly, M. A. Lowery, L. G. T. Morris, A. M. Omuro, N. Raj, P. Razavi, A. N. Shoushtari, N. Shukla, T. E. Soumerai, A. M. Varghese, R. Yaeger, J. Coleman, B. Bochner, G. J. Riely, L. B. Saltz, H. I. Scher, P. J. Sabbatini, M. E. Robson, D. S. Klimstra, B. S. Taylor, J. Baselga, N. Schultz, D. M. Hyman, M. E. Arcila, D. B. Solit, M. Ladanyi, M. F. Berger, Mutational landscape of metastatic cancer revealed from prospective clinical sequencing of 10,000 patients. *Nat. Med.* **23**, 703–713 (2017).
28. D. Miao, C. A. Margolis, N. I. Vokes, D. Liu, A. Taylor-Weiner, S. M. Wankowicz, D. Adeegbe, D. Keliher, B. Schilling, A. Tracy, M. Manos, N. G. Chau, G. J. Hanna, P. Polak, S. J. Rodig, S. Signoretti, L. M. Sholl, J. A. Engelman, G. Getz, P. A. Jänne, R. I. Haddad, T. K. Choueiri, D. A. Barbie, R. Haq, M. M. Awad, D. Schadendorf, F. S. Hodi, J. Bellmunt, K.-K. Wong, P. Hammerman, E. M. Van Allen, Genomic correlates of response to immune checkpoint blockade in microsatellite-stable solid tumors. *Nat. Genet.* **50**, 1271–1281 (2018).
29. ICGC/TCGA Pan-Cancer Analysis of Whole Genomes Consortium, Pan-cancer analysis of whole genomes. *Nature* **578**, 82–93 (2020).
30. Cancer Genome Atlas Research Network, Comprehensive molecular characterization of clear cell renal cell carcinoma. *Nature* **499**, 43–49 (2013).
31. V. H. Haase, The VHL tumor suppressor: Master regulator of HIF. *Curr. Pharm. Des.* **15**, 3895–3903 (2009).
32. N. Varshney, A. A. Kebede, H. Owusu-Dapaah, J. Lather, M. Kaushik, J. S. Bhullar, A review of Von Hippel-Lindau syndrome. *J. Kidney Cancer VHL* **4**, 20–29 (2017).
33. L. Masclef, O. Ahmed, B. Estavoyer, B. Larrivée, N. Labrecque, A. Nijnik, E. B. Affar, Roles and mechanisms of BAP1 deubiquitinase in tumor suppression. *Cell Death Differ.* **28**, 606–625 (2021).
34. A. P. Szczepanski, L. Wang, Emerging multifaceted roles of BAP1 complexes in biological processes. *Cell Death Discov.* **7**, 20 (2021).
35. J. C. Scheuermann, A. G. de Ayala Alonso, K. Oktaba, N. Ly-Hartig, R. K. McGinty, S. Fraterman, M. Wilm, T. W. Muir, J. Müller, Histone H2A deubiquitinase activity of the polycomb repressive complex PR-DUB. *Nature* **465**, 243–247 (2010).
36. Q. Wu, M. Wright, M. M. Gogol, W. D. Bradford, N. Zhang, A. A. Bazzini, Translation of small downstream ORFs enhances translation of canonical main open reading frames. *EMBO J.* **39**, e104763 (2020).
37. K. L. Hickey, K. Dickson, J. Z. Cogan, J. M. Replogle, M. Schoof, K. N. D'Orazio, N. K. Sinha, J. A. Hussmann, M. Jost, A. Frost, R. Green, J. S. Weissman, K. K. Kostova, GIGYF2 and 4EHP inhibit translation initiation of defective messenger RNAs to assist ribosome-associated quality control. *Mol. Cell* **79**, 950–962.e6 (2020).
38. S. Juszkiewicz, G. Slodkowicz, Z. Lin, P. Freire-Pritchett, S.-Y. Peak-Chew, R. S. Hegde, Ribosome collisions trigger cis-acting feedback inhibition of translation initiation. *eLife* **9**, e60038 (2020).
39. S. Shao, A. Brown, B. Santhanam, R. S. Hegde, Structure and assembly pathway of the ribosome quality control complex. *Mol. Cell* **57**, 433–444 (2015).
40. S. Mazumder, P. J. Higgins, R. Samarakoon, Downstream targets of VHL/HIF-α signaling in renal clear cell carcinoma progression: Mechanisms and therapeutic relevance. *Cancers (Basel)* **15**, 1316 (2023).
41. J. Hu, P. Tan, M. Ishihara, N. A. Bayley, S. Schokrpur, J. G. Reynoso, Y. Zhang, R. J. Lim, C. Dumitras, L. Yang, S. M. Dubinett, P. S. Jat, J. Van Snick, J. Huang, A. I. Chin, R. M. Prins, T. G. Graeber, H. Xu, L. Wu, Tumor heterogeneity in VHL drives metastasis in clear cell renal cell carcinoma. *Signal Transduct. Target. Ther.* **8**, 155 (2023).
42. S. Alberti, A. A. Hyman, Biomolecular condensates at the nexus of cellular stress, protein aggregation disease and ageing. *Nat. Rev. Mol. Cell Biol.* **22**, 196–213 (2021).
43. J. S. Kesner, Z. Chen, P. Shi, A. O. Aparicio, M. R. Murphy, Y. Guo, A. Trehan, J. E. Lipponen, Y. Recinos, N. Myeku, X. Wu, Noncoding translation mitigation. *Nature* **617**, 395–402 (2023).
44. A. Schoenfeld, E. J. Davidowitz, R. D. Burk, A second major native von Hippel-Lindau gene product, initiated from an internal translation start site, functions as a tumor suppressor. *Proc. Natl. Acad. Sci. U.S.A.* **95**, 8817–8822 (1998).
45. P. Hascoet, F. Chesnel, F. Jouan, C. Le Goff, A. Couturier, E. Darrigrand, F. Mahe, N. Rioux-Leclercq, X. Le Goff, Y. Arlot-Bonnemains, The pVHL172 isoform is not a tumor suppressor and up-regulates a subset of pro-tumorigenic genes including *TGFB1* and *MMP13*. *Oncotarget* **8**, 75989–76002 (2017).
46. A. Fukao, T. Tomohiro, T. Fujiwara, Translation initiation regulated by RNA-binding protein in mammals: The modulation of translation initiation complex by trans-acting factors. *Cells* **10**, 1711 (2021).
47. M. Caudron-Herger, R. E. Jansen, E. Wassmer, S. Diederichs, RBP2GO: A comprehensive pan-species database on RNA-binding proteins, their interactions and functions. *Nucleic Acids Res.* **49**, D425–D436 (2021).
48. R. She, J. Luo, J. S. Weissman, Translational fidelity screens in mammalian cells reveal eIF3 and eIF4G2 as regulators of start codon selectivity. *Nucleic Acids Res.* **51**, 6355–6369 (2023).
49. L. A. Passmore, T. M. Schmeing, D. Maag, D. J. Applefield, M. G. Acker, M. A. Algire, J. R. Lorsch, V. Ramakrishnan, The eukaryotic translation initiation factors eIF1 and eIF1A induce an open conformation of the 40S ribosome. *Mol. Cell* **26**, 41–50 (2007).
50. D. J. Grove, P. J. Russell, M. G. Kearse, To initiate or not to initiate: A critical assessment of eIF2A, eIF2D, and MCT-1·DENR to deliver initiator tRNA to ribosomes. *Wiley Interdiscip Rev. RNA* **15**, e1833 (2024).
51. J. L. Llácer, T. Hussain, J. Dong, L. Villamayor, Y. Gordiyenko, A. G. Hinnebusch, Large-scale movement of eIF3 domains during translation initiation modulate start codon selection. *Nucleic Acids Res.* **49**, 11491–11511 (2021).
52. T. Egorova, N. Biziaev, A. Shuvalov, E. Sokolova, S. Mukba, K. Evmenov, M. Zotova, A. Kushchenko, E. Shuvalova, E. Alkalaeva, eIF3j facilitates loading of release factors into the ribosome. *Nucleic Acids Res.* **49**, 11181–11196 (2021).
53. C. U. T. Hellen, Translation termination and ribosome recycling in eukaryotes. *Cold Spring Harb. Perspect. Biol.* **10**, a032656 (2018).
54. P. Beznosková, S. Wagner, M. E. Jansen, T. von der Haar, L. S. Valášek, Translation initiation factor eIF3 promotes programmed stop codon readthrough. *Nucleic Acids Res.* **43**, 5099–5111 (2015).
55. R. R. Lonser, G. M. Glenn, M. Walther, E. Y. Chew, S. K. Libutti, W. M. Linehan, E. H. Oldfield, von Hippel-Lindau disease. *Lancet* **361**, 2059–2067 (2003).
56. M. L. M. Binderup, E. Budtz-Jørgensen, M. L. Bisgaard, Risk of new tumors in von Hippel-Lindau patients depends on age and genotype. *Genet. Med.* **18**, 89–97 (2016).
57. A. D. Sorrell, S. Lee, C. Stolle, J. Ellenhorn, A. Grix, W. G. Kaelin, J. N. Weitzel, Clinical and functional properties of novel VHL mutation (X214L) consistent with type 2A phenotype and low risk of renal cell carcinoma. *Clin. Genet.* **79**, 539–545 (2011).

58. J. H. Kim, M. J. Kim, S. H. Kong, S. J. Kim, H. Kang, C. S. Shin, S. S. Park, K. E. Lee, M.-W. Seong, Characteristics of germline mutations in Korean patients with pheochromocytoma/paraganglioma. *J. Med. Genet.* **59**, 56–64 (2022).
59. A. H. Bauer, D. W. Basta, J. L. Hornick, F. Dong, Loss of function SMAD4 nonstop mutations in human cancer. *Histopathology* **82**, 1098–1104 (2023).
60. R. Nussinov, C.-J. Tsai, H. Jang, Why are some driver mutations rare? *Trends Pharmacol. Sci.* **40**, 919–929 (2019).
61. F. Martínez-Jiménez, F. Muiños, I. Sentís, J. Deu-Pons, I. Reyes-Salazar, C. Arnedo-Pac, L. Mularoni, O. Pich, J. Bonet, H. Kranas, A. Gonzalez-Perez, N. Lopez-Bigas, A compendium of mutational cancer driver genes. *Nat. Rev. Cancer* **20**, 555–572 (2020).
62. M. Carbone, H. Yang, H. I. Pass, T. Krausz, J. R. Testa, G. Gaudino, BAP1 and cancer. *Nat. Rev. Cancer* **13**, 153–159 (2013).
63. N. Akimitsu, J. Tanaka, J. Pelletier, Translation of nonSTOP mRNA is repressed post-initiation in mammalian cells. *EMBO J.* **26**, 2327–2338 (2007).
64. C. Razafinjatovo, S. Bihr, A. Mischo, U. Vogl, M. Schmidinger, H. Moch, P. Schraml, Characterization of VHL missense mutations in sporadic clear cell renal cell carcinoma: Hotspots, affected binding domains, functional impact on pVHL and therapeutic relevance. *BMC Cancer* **16**, 638 (2016).
65. L. Yang, Z. Zhao, S. Zhao, C. Chen, X. Cong, Z. Li, M. Ren, The clinicopathological significance of epigenetic silencing of VHL promoter and renal cell carcinoma: A meta-analysis. *Cell. Physiol. Biochem.* **40**, 1465–1472 (2016).
66. L. Favazza, D. A. Chitale, R. Barod, C. G. Rogers, S. Kalyana-Sundaram, N. Palanisamy, N. S. Gupta, S. R. Williamson, Renal cell tumors with clear cell histology and intact VHL and chromosome 3p: A histological review of tumors from the Cancer Genome Atlas database. *Mod. Pathol.* **30**, 1603–1612 (2017).
67. I. J. Frew, H. Moch, A clearer view of the molecular complexity of clear cell renal cell carcinoma. *Annu. Rev. Pathol.* **10**, 263–289 (2015).
68. A. J. Pantuck, J. An, H. Liu, M. B. Rettig, NF-κB–dependent plasticity of the epithelial to mesenchymal transition induced by *Von Hippel-Lindau* inactivation in renal cell carcinomas. *Cancer Res.* **70**, 752–761 (2010).
69. D. Matsuda, V. P. Mauro, Determinants of initiation codon selection during translation in mammalian cells. *PLOS ONE* **5**, e15057 (2010).
70. T. E. Dever, I. P. Ivanov, A. G. Hinnebusch, Translational regulation by uORFs and start codon selection stringency. *Genes Dev.* **37**, 474–489 (2023).
71. J. B. Querido, M. Sokabe, S. Kraatz, Y. Gordiyenko, J. M. Skehel, C. S. Fraser, V. Ramakrishnan, Structure of a human 48 *S* translational initiation complex. *Science* **369**, 1220–1227 (2020).
72. H. K. Kini, I. M. Silverman, X. Ji, B. D. Gregory, S. A. Liebhaber, Cytoplasmic poly (A) binding protein-1 binds to genomically encoded sequences within mammalian mRNAs. *RNA* **22**, 61–74 (2016).
73. R. J. Jackson, C. U. T. Hellen, T. V. Pestova, Termination and post-termination events in eukaryotic translation. *Adv. Protein Chem. Struct. Biol.* **86**, 45–93 (2012).
74. S. E. Wells, P. E. Hillner, R. D. Vale, A. B. Sachs, Circularization of mRNA by eukaryotic translation initiation factors. *Mol. Cell* **2**, 135–140 (1998).
75. G. Minervini, G. M. Mazzotta, A. Masiero, E. Sartori, S. Corrà, E. Potenza, R. Costa, S. C. E. Tosatto, Isoform-specific interactions of the von Hippel-Lindau tumor suppressor protein. *Sci. Rep.* **5**, 12605 (2015).
76. C. A. Schneider, W. S. Rasband, K. W. Eliceiri, NIH Image to ImageJ: 25 years of image analysis. *Nat. Methods* **9**, 671–675 (2012).

Acknowledgments: We thank D. Helm and M. Schneider from the DKFZ Proteomics Core Facility as well as the Lighthouse Core Facility at the University Hospital Freiburg. We thank all patients for participation in the Freiburg VHL Registry and the FREEZE-Biobank Center for Biobanking (University Medical Center Freiburg). We also thank H. Neumann for contribution to the establishment of the Freiburg VHL Registry. We thank T. Saikia, Computer Vision Group, University of Freiburg, for support in data analysis. Last, we would like to thank all members of the Diederichs laboratory for helpful discussion and support as well as M. Klein for excellent technical assistance. **Funding:** This work was supported by the German Research Foundation (DFG) through grant Di 1421/9-2 to S.Di. and Project-ID 431984000 - SFB 1453 to S.Di., A.Ga., I.J.F., and E.N.-H. S.Dh. is recipient of the DBT/Wellcome Trust India Alliance Fellowship (IA/I/22/2/506497).
Author contributions: Conceptualization: J.P., I.J.F., and S.Di. Investigation: J.P., A.Ga., A.Gh., D.M., C.V., F.K., and E.N.-H. Methodology: J.P., A.Gh., S.Dh., D.M., I.J.F., and S.Di. Formal analysis: J.P., A.Ga., and D.M. Visualization: J.P., A.Ga., C.V., and S.Di. Validation: J.P., M.R., A.Gh., D.M., and C.V. Data curation: J.P. and C.V. Resources: A.Ga., C.V., I.J.F., F.K., E.N.-H., and A.S. Supervision: A.S. and S.Di. Project administration: A.S. and S.Di. Funding acquisition: A.Ga., E.N.-H., and S.Di. Writing—original draft: J.P. Writing—review and editing: J.P., A.Ga., A.Gh., S.Dh., C.V., I.J.F., F.K., A.S., and S.Di.
Competing interests: S.Di. is a co-owner of siTOOLs Biotech, Martinsried, Germany, and supported by a sponsored research agreement from BioMarin Pharmaceutical Inc., unrelated to this work. All other authors declare that they have no competing interests. **Data and materials availability:** The nonstop extension sequences used in this study were obtained from and are provided in the NonStopDB database accessible at https://NonStopDB.dkfz.de. The proteomic raw data have been deposited at the ProteomeXchange Consortium via the PRIDE partner repository and can be accessed using the dataset identifier PXD053175. Newly created plasmids and cell lines are available upon request from the corresponding author. All other data needed to evaluate the conclusions in the paper are present in the paper and/or the Supplementary Materials.

Submitted 10 July 2024
Accepted 13 January 2025
Published 12 February 2025
10.1126/sciadv.adr6375